BIOCHEMISTRY
including biophysical chemistry & molecular biology
Article

Biochemistry **2010,** *49,* 8197–8212 8197
DOI: 10.1021/bi100828r

Double Duty for a Conserved Glutamate in Pyruvate Decarboxylase: Evidence of the Participation in Stereoelectronically Controlled Decarboxylation and in Protonation of the Nascent Carbanion/Enamine Intermediate[†,‡]

Danilo Meyer,[§,∥] Piotr Neumann,[∥,#] Christoph Parthier,[∥] Rudolf Friedemann,[⊥] Natalia Nemeria,[@] Frank Jordan,[@] and Kai Tittmann*[,§,∥]

[§]*Albrecht-von-Haller-Institute for Plant Sciences and Göttingen Center for Molecular Biosciences, Georg-August-University Göttingen, Ernst-Caspari-Haus, Justus-von-Liebig-Weg 11, D-37077 Göttingen, Germany,* [∥]*Institute of Biochemistry and Biotechnology, Martin-Luther-University Halle-Wittenberg, Kurt-Mothes-Strasse 3, D-06120 Halle/Saale, Germany,* [⊥]*Institute of Organic Chemistry, Martin-Luther-University Halle-Wittenberg, Kurt-Mothes-Strasse 3, D-06120 Halle/Saale, Germany, and* [@]*Department of Chemistry, Rutgers University, Newark, New Jersey 07102.* [#]*Current address: Institute for Microbiology and Genetics, Georg-August-University Göttingen, Göttingen, Germany.*

Received May 25, 2010; Revised Manuscript Received August 16, 2010

ABSTRACT: Pyruvate decarboxylase (PDC) catalyzes the nonoxidative decarboxylation of pyruvate into acetaldehyde and carbon dioxide and requires thiamin diphosphate (ThDP) and a divalent cation as cofactors. Recent studies have permitted the assignment of functional roles of active site residues; however, the underlying reaction mechanisms of elementary steps have remained hypothetical. Here, a kinetic and thermodynamic single-step analysis in conjunction with X-ray crystallographic studies of PDC from *Zymomonas mobilis* implicates active site residue Glu473 (located on the *re*-face of the ThDP thiazolium nucleus) in facilitating both decarboxylation of 2-lactyl-ThDP and protonation of the 2-hydroxyethyl-ThDP carbanion/enamine intermediate. Variants carrying either an isofunctional (Glu473Asp) or isosteric (Glu473Gln) substitution exhibit a residual catalytic activity of less than 0.1% but accumulate different intermediates at the steady state. Whereas the predecarboxylation intermediate 2-lactyl-ThDP is accumulated in Glu473Asp because of a 3000-fold slower decarboxylation compared to that of the wild-type enzyme, Glu473Gln is not impaired in decarboxylation but generates a long-lived 2-hydroxyethyl-ThDP carbanion/enamine postdecarboxylation intermediate. CD spectroscopic analysis of the protonic and tautomeric equilibria of the cocatalytic aminopyrimidine part of ThDP indicates that an acidic residue is required at position 473 for proper substrate binding. Wild-type PDC and the Glu473Asp variant bind the substrate analogue acetylphosphinate with the same affinity, implying a similar stabilization of the predecarboxylation intermediate analogue on the enzyme, whereas Glu473Gln fails to bind the analogue. The X-ray crystallographic structure of 2-lactyl-ThDP trapped in the decarboxylation-deficient variant Glu473Asp reveals a common stereochemistry of the intermediate C2α stereocenter; however, the scissile C2α−C(carboxylate) bond deviates by ∼25−30° from the perpendicular "maximum overlap" orientation relative to the thiazolium ring plane as commonly observed in ThDP enzymes. Because a reactant-state stabilization of the predecarboxylation intermediate can be excluded to account for the slower decarboxylation, the data suggest a strong stereoelectronic effect for the transition state of decarboxylation as supported by additional DFT studies on models. To the best of our knowledge, this is a very rare example in which the magnitude of a stereoelectronic effect could be experimentally estimated for an enzymatic system. Given that variant Glu473Gln is not decarboxylation-deficient, electrostatic stress can be excluded as a driving force for decarboxylation. The apparent dual function of Glu473 further suggests that decarboxylation and protonation of the incipient carbanion are committed and presumably proceed in the same transition state.

Pyruvate decarboxylase (PDC,[1] EC 4.1.1.1) is a thiamin diphosphate-dependent enzyme that carries out the nonoxidative decarboxylation of pyruvate yielding acetaldehyde and carbon dioxide (eq 1) as a central reaction of alcoholic fermentation in yeast, germinating seeds, and some microorganisms such as *Zymomonas mobilis* or *Acetobacter pasteurianus* (*1*, *2*).

$$CH_3-CO-CO_2^- + H_2O \rightarrow CH_3-CHO + CO_2 + OH^- \quad (1)$$

[†]This work was supported in part by Grant 0126FP/0705M from the Ministry of Education at Saxony-Anhalt and the DFG-funded Göttingen Graduate School for Neurosciences and Molecular Biosciences (both to K.T.). At Rutgers University, the research was supported by National Institutes of Health Grant GM050380 (to F.J.).

[‡]The refined model and corresponding structure factor amplitudes have been deposited in the Protein Data Bank of the Research Collaboratory for Structural Biology as entry 3OE1.

*To whom correspondence should be addressed. Phone: +49-551-3914430. Fax: +49-551-395749. E-mail: ktittma@gwdg.de.

[1]Abbreviations: PDC, pyruvate decarboxylase; *Zm*PDC, pyruvate decarboxylase from *Zymomonas mobilis;* *Sc*PDC, pyuvate decarboxylase from *Saccharomyces cerevisiae*; BFDC, benzoylformate decarboxylase; POX, pyruvate oxidase; ThDP, thiamin diphosphate; ThDP$^-$, carbanion form of ThDP; LThDP, 2-lactyl-ThDP; HEThDP, 2-(1-hydroxyethyl)-ThDP; HEThDP$^-$, carbanion/enamine form of HEThDP; AcP, acetylphosphinate; MAP, methyl acetylphosphonate; PDB, Protein Data Bank; rmsd, root-mean-square deviation.

Published on Web 08/17/2010

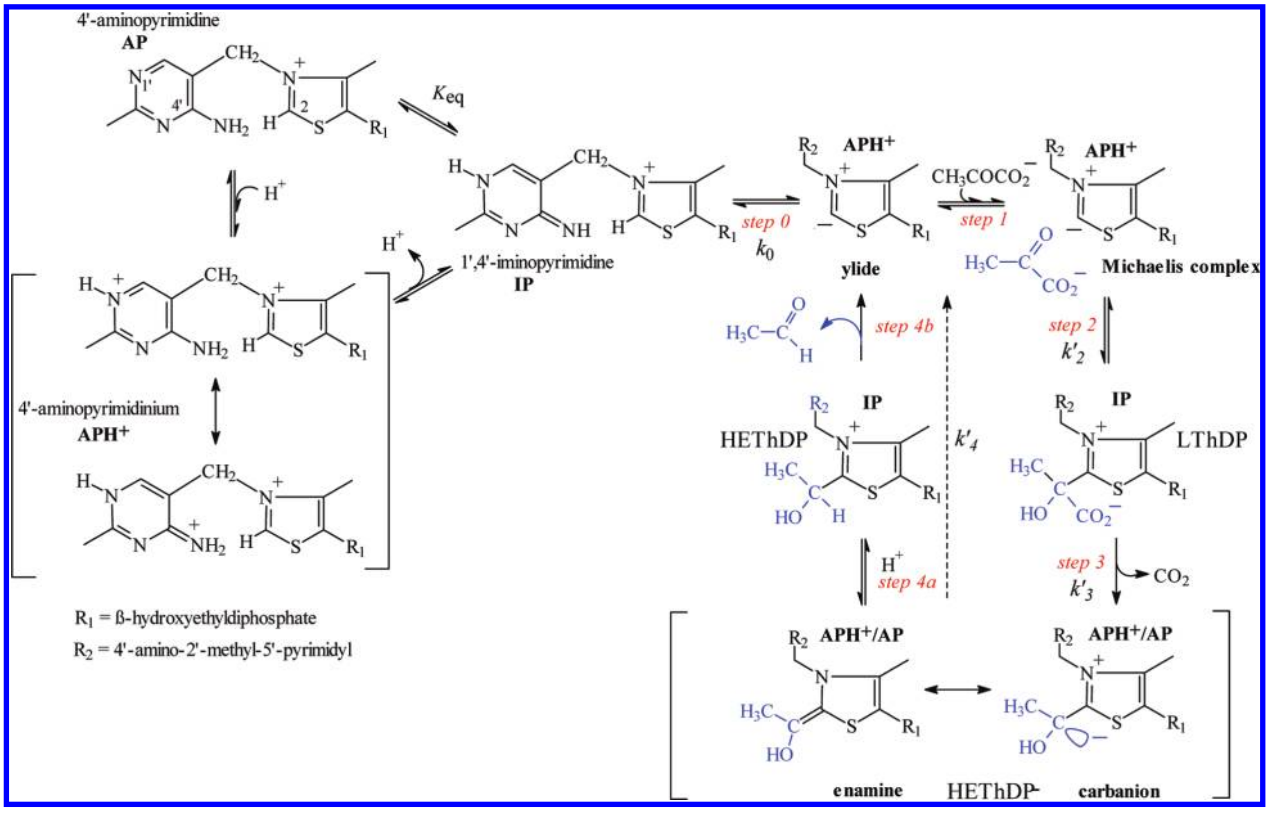

FIGURE 1: Catalytic cycle of *Zm*PDC with intermediates and elementary catalytic steps identified.

As opposed to PDCs from yeasts and plants, the bacterial enzymes such as PDC from *Z. mobilis* (*Zm*PDC) are constitutively activated and not subject to homotropic substrate activation. In that way, they are kinetically well-suited model systems for studying the molecular reaction mechanism in the absence of additional complex conformational equilibria.

The catalytic sequence of PDC can be subdivided into several elementary steps and involves numerous reaction intermediates (Figure 1). After formation of the cofactor reactive ylide form (step 0) and of the substrate Michaelis complex (step 1), the ThDP C2 carbanion attacks the substrate carbonyl in a nucleophilic manner to yield the tetrahedral predecarboxylation intermediate 2-lactyl-ThDP (LThDP) (step 2). Decarboxylation of LThDP gives the resonant carbanion/enamine forms of the post-decarboxylation intermediate 2-hydroxyethyl-ThDP (HEThDP$^-$) (step 3). Protonation at C2α of HEThDP$^-$ (step 4a) yields its conjugate acid HEThDP. Finally, ionization of the C2α-OH group of HEThDP and cleavage of its C2−C2α bond lead to the liberation of the product acetaldehyde (step 4b).

The occurrence and quantitative distribution of these on-pathway intermediates in PDC catalysis could be demonstrated by NMR and circular dichroism (CD) spectroscopy (*3*−*5*). In agreement with ^{13}C kinetic isotope effect studies (*6*, *7*), this analysis revealed decarboxylation of LThDP and acetaldehyde liberation to be partially rate-determining for catalysis, whereas cofactor activation and carbonyl addition of bound pyruvate to ThDP proceed at least 1 order of magnitude faster. CD spectroscopic studies on PDC from *Saccharomyces cerevisiae* (*Sc*PDC) and other ThDP-dependent enzymes indicated that the cocatalytic aminopyrimidine moiety of enzyme-bound ThDP exists in different protonic and tautomeric states (Figure 1), all of which are catalytically important and thermodynamically accessible at the pH optimum of a given ThDP enzyme (*8*). Whereas tetrahedral intermediates (LThDP and HEThDP in PDC) predominantly stabilize the 1′,4′-iminotautomeric form (IP) of the aminopyrimidine ring, the 4′-amino (AP) and 1′,4′-aminopyrimidinium (APH$^+$) forms are supposed to be stabilized in the resting state, in the substrate Michaelis complex, and in the carbanion/enamine intermediate (HEThDP$^-$ in PDC) (*4*, *9*).

The structures of *Zm*PDC and *Sc*PDC in the resting state were determined by X-ray crystallography in the 1990s (*10*, *11*), but to date, there is no direct structural information available concerning covalent reaction intermediates in PDC catalysis. However, recent crystallographic studies on substrate/ThDP intermediates in the related enzyme pyruvate oxidase (POX) shed light on the stereochemical course of substrate binding and processing in ThDP-dependent enzymes, which appears to be a conserved feature in this enzyme superfamily (*12*−*14*). Modeling of the (*S*)-LThDP and (*E*)-HEThDP enamine intermediates observed in POX into the active site of *Zm*PDC suggests a three-center substrate binding motif that consists of a "carboxylate subsite" (Glu473, Asp27, His113, and Tyr290 in *Zm*PDC), a "carbonyl/α-hydroxyl subsite" (His114, Gly413, and 4′-NH_2 of ThDP), and a "methyl substituent subsite" (Thr388 and Ile472) (Figure 2). Consistent with the structural model, earlier kinetic and mutagenesis studies on both *Sc*PDC and *Zm*PDC identified residues of the carboxylate subsite to be essential for decarboxylation and product release (Glu473, Asp27, and His113 in *Zm*PDC), whereas functional groups of the carbonyl/α-hydroxyl subsite (4′-NH_2 of ThDP and Glu50) were found to be involved in carbonyl addition and/or elimination of pyruvate and acetaldehyde, with the aminopyrimidine portion of ThDP presumably acting as a general acid/base catalyst (*3*, *15*−*17*). The modeled intermediate structures suggest a crucial role for Glu473 for both decarboxylation of LThDP and protonation of the HEThDP enamine. In the predecarboxylation state (Figure 2A), the γ-carboxyl

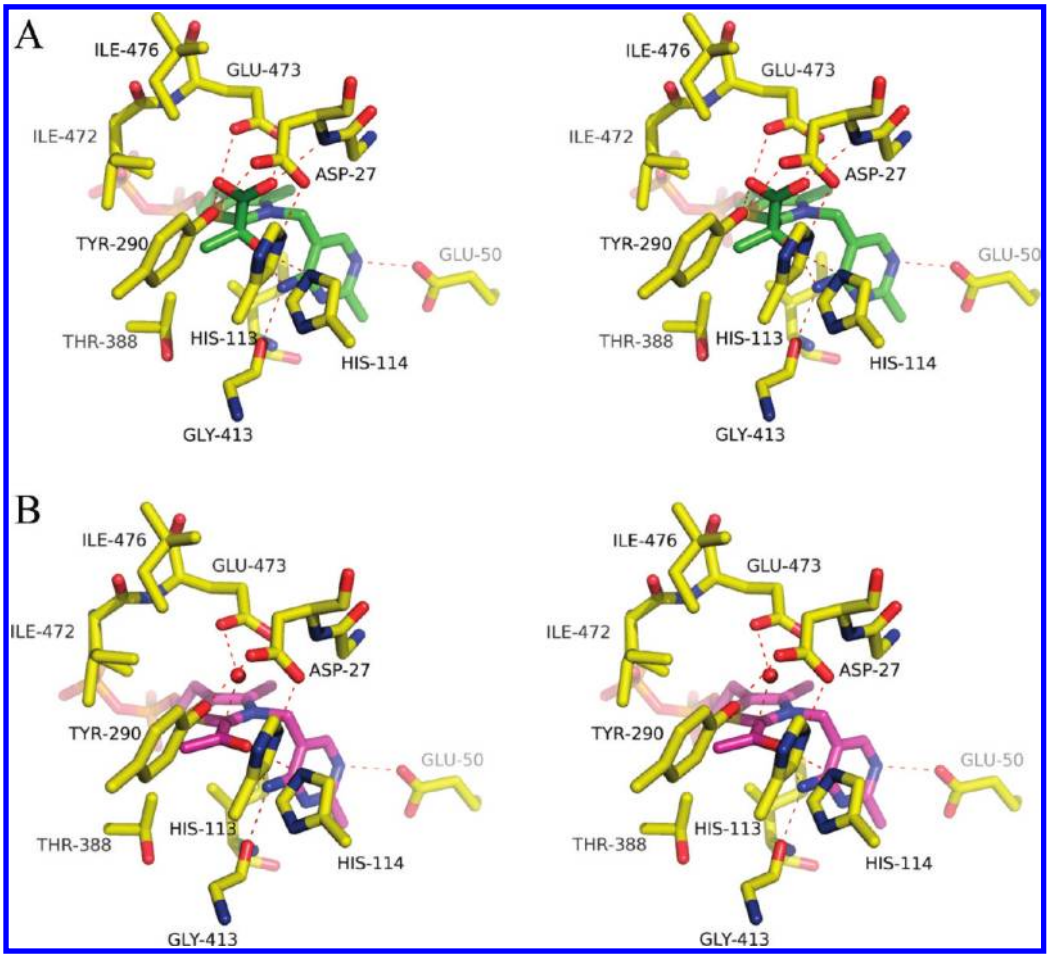

FIGURE 2: Structural model of predecarboxylation intermediate LThDP (A) and of postdecarboxylation intermediate HEThDP carbanion/enamine (B) at the active center of *Zm*PDC in stereoview. Dotted lines indicate hydrogen bonding interactions (< 3.2 Å contacts). The X-ray structures of LThDP and HEThDP carbanion/enamine intermediates both independently trapped in the related enzyme pyruvate oxidase (*12*) were modeled into the active site of wild-type *Zm*PDC (PDB entry 1ZPD) by superposing the cofactor atoms.

group of Glu473 would be positioned face to face with the carboxylate moiety of LThDP. When ionized, Glu473 could facilitate decarboxylation of LThDP by imposing "electrostatic stress" on the carboxylate leaving group. Alternatively, Glu473 may be uncharged and thus serve to orient the carboxylate leaving group of LThDP via a hydrogen bonding interaction such that the scissile C2α−C(carboxylate) bond would be directed perpendicular to the thiazolium ring plane. Such a conformation would ensure a maximum overlap between the incipient electron pair at C2α and the π-electrons of the thiazolium ring. In the postdecarboxylation state, Glu473 could act as a general acid to protonate the carbanion/enamine intermediate (provided it is protonated at this reaction state), presumably involving a bridging water molecule observed as a placeholder in the resting state of *Zm*PDC (Figure 2B), and other side chains such as Asp27 and His113, which were already shown to form, jointly with Glu473, a functional triad for acetaldehyde liberation.

To elucidate the functional role of Glu473 for PDC catalysis and, in a broader sense, to gather information about the chemical reaction mechanism and potential driving forces of LThDP decarboxylation and protonation of the subsequently formed carbanion/enamine intermediate, we have functionally and structurally examined single-site variants of *Zm*PDC with isofunctional (Glu473Asp) and isosteric (Glu473Gln) substitutions, including a detailed kinetic and thermodynamic analysis of elementary reaction steps in conjunction with X-ray crystallographic studies on reaction intermediates.

MATERIALS AND METHODS

Chemicals and Reagents. Alcohol dehydrogenase from *S. cereviseae*, D_2O (99.9%), ThDP, sodium pyruvate, and NADH were purchased from Sigma-Aldrich Chemie GmbH. All other chemicals were obtained from VWR International GmbH, Sigma-Aldrich Chemie GmbH, Carl Roth GmbH, and Appli-Chem GmbH. Quartz doubly distilled water was used throughout the experiments.

Synthesis of Pyruvate Analogues Acetylphosphinate and Methyl Acetylphosphonate. Chemical synthesis of substrate analogue acetylphosphinate (APh) was conducted according to the procedure given in ref *18*. Methyl phosphonousdichloride was purchased from Aldrich and was used without further purification. NaI was dried at 70 °C under 0.1 mm/Hg overnight. Dry acetone was prepared with dry NaI according to literature procedures. Methyl acetylphosphonate (MAP) was synthesized using trimethylphosphite and acetylchloride as reagents according to the method described in ref *19*. The purity and correct synthesis of both compounds were confirmed by NMR spectroscopy and mass spectrometry.

Expression and Purification of PDC from Z. mobilis. *Escherichia coli* SG13009 cells carrying plasmid pZY134b that encodes wild-type PDC from *Z. mobilis* were cultivated at 30 °C

in 2YT medium supplemented with 100 μg/mL ampicillin and 50 μg/mL kanamycin. Gene expression was induced at an OD_{600} of ~0.5−0.8 by addition of 1 mM IPTG, and cells were grown for an additional 14−17 h at 30 °C. Cells were then harvested by centrifugation (20 min at 4000*g* and 4 °C), shock-frozen in liquid nitrogen, and stored at −80 °C. For enzyme purification, cells were thawed on ice and resuspended in low-salt buffer [0.01 M MES (pH 6.5), 0.1 mM ThDP, and 1 mM $MgSO_4$]. Thereafter, cells were disrupted by repeated passages in a French press (Gaulin, APV Homogenizer GmbH). Cell debris was separated from the soluble fraction by centrifugation (30 min at 4 °C and 59000*g*). DNA in the supernatant was removed by precipitation with 0.8% (w/v) streptomycin or by DNase I digestion (5 μg/mL DNase and 1 mM $MgCl_2$ for 45 min at 8 °C). PDC was initially enriched by fractional ammonium sulfate precipitation [20 and 43% (w/v)]. The pellet of the second precipitation step was gently dissolved in ~10 mL of low-salt buffer (see above) and exhaustively dialyzed against the same buffer overnight. After dialysis, the protein solution was applied to an anion exchange column [Fractogel EMD TMAE (S), Merck, 30 mL batch volume] previously equilibrated with low-salt buffer. *Zm*PDC was eluted from the column using a linear gradient from 0 to 40% high-salt buffer [0.01 M MES (pH 6.5), 0.1 mM ThDP, 1 mM $MgSO_4$, and 100 mM $(NH_4)_2SO_4$] over a total volume of 150 mL. The fractions containing *Zm*PDC were pooled and concentrated by ultrafiltration in centrifugal concentrators with a molecular mass cutoff of 30 kDa (VIVASPIN 15R, 2600*g* and 4 °C). For final purification and concomitant buffer exchange, the protein solution was applied to a gel filtration column (Superdex 200 16/60, GE Healthcare, 120 mL batch volume) equilibrated with 50 mM MES/NaOH (pH 6.0), 100 μM ThDP, and 1 mM Mg^{2+}.

*Zm*PDC variants Glu473Asp and Glu473Gln were expressed in *E. coli* JM109 cells using plasmid pPLZM as a vector that contains a heat-inducible promoter (*15*). Cells were cultivated in 2YT medium containing 100 μg/mL ampicillin at 30 °C, and expression was induced via a rapid increase in temperature to 42 °C. Cells were grown for 3−4 h at 42 °C and then harvested by centrifugation (20 min at 4000*g* and 4 °C). All remaining purification steps were conducted as detailed above for wild-type *Zm*PDC.

Steady-State Kinetic Analysis. The enzymatic activity of *Zm*PDC was determined spectrophotometrically at 366 nm in a coupled optical test employing NADH (ε_{366} = 3400 M^{-1} cm^{-1}) and alcohol dehydrogenase as an auxiliary enzyme. Activity measurements were conducted in 50 mM MES buffer (pH 6.0) supplemented with 1 mM $MgSO_4$ and 100 μM ThDP at 30 °C and further containing 0.3 mM NADH and 0.15 unit/mL alcohol dehydrogenase. The catalytic constants were calculated by fitting the experimental data to the Michaelis−Menten equation. The pH dependence of catalytic activity was analyzed as previously described (*20*).

Analysis of Protonic−Tautomeric Equilibria of Enzyme-Bound ThDP and Acetylphosphinate Binding to ZmPDC Using Circular Dichroism Spectroscopy. Earlier work at Rutgers University had established that the aminopyrimidine ring of enzyme-bound ThDP gives rise to CD signals as selective probes for the different chemical states: the 4′-amino form (AP), the 1′,4′-imino form (IP), and the aminopyrimidinium form (APH^+) (see Figure 1) (*8*). The IP form of the enzyme-bound cofactor gives rise to a positive CD band at 300−310 nm, while a negative band at 320−330 nm was suggested to pertain to the AP form (an intramolecular charge transfer complex between the aminopyrimidine as the donor and the thiazolium as the acceptor). The APH^+ form could not be unambigously identified by CD spectroscopy, although a UV band is expected at ~260 nm.

To study the pH dependence of the internal protonic equilibria of enzyme-bound ThDP in *Zm*PDC, the pH of the protein solution [2 mg/mL in two-component buffer consisting of 20 mM MES and 20 mM phosphate (pH 6.0) supplemented with 100 μM ThDP and 1 mM Mg^{2+}] was adjusted via gentle addition of Tris base (pH 11) using a sympHony pH electrode (VWR). Circular dichroism spectra were recorded on a Chirascan CD spectrometer from Applied Photophysics (Leatherhead, U.K.) in a 10 mm path length cell in the near-UV wavelength region (250−500 nm) at 20 °C. The pK_a was estimated by fitting the log of the buffer-corrected CD signal at 300 nm versus pH according to eq 2 that accounts for a single ionizing group

$$\log \Theta_{300} = \log \Theta_{300}{}^{\max} - \log(1 + 10^{pK_a - x}) \quad (2)$$

where x is the pH. When negative CD signals were observed, difference spectra were used for quantitative analysis with the signal at the lowest pH as a reference.

To selectively analyze substrate binding, we employed acetylphosphinate (AcP) and methyl acetylphosphonate (MAP) as electrostatic analogues of pyruvate (*19*, *21*). It was demonstrated for numerous ThDP enzymes that these compounds add to C2 of enzyme-bound ThDP in a manner analogous to that of pyruvate, yielding stable tetrahedral predecarboxylation intermediate analogues, which are not further processed (*14*). Because initial experiments indicated that neither wild-type *Zm*PDC nor its variants bind MAP even after prolonged reaction times (several hours), AcP was used for quantitative analysis. AcP was sequentially titrated to 2 mg/mL *Zm*PDC (two-component buffer as used for pH studies adjusted to pH 6.0) over a concentration range from 0 to 12 mM (final concentration). After each titration step, the binding equilibrium was allowed to be established for 10 min. Subsequently, CD spectra (Chirascan CD spectrometer) were recorded in the wavelength range of 295−400 nm at 20 °C using an optical path length of 1 cm. All spectra were corrected for buffer contributions and concomitant dilution in the titration series.

For quantitative analysis, the CD signal intensities of the IP and AP bands were plotted versus AcP concentration. Apparent dissociation constants ($K_D{}^{app}$) were calculated by fitting the data to a hyperbolic function using SigmaPlot and KaleidaGraph.

$$\Theta = \Theta^0 + \frac{\Theta^{max}[AcP]}{K_D{}^{app} + [AcP]} \quad (3)$$

where Θ is the observed CD signal at a given wavelength, Θ^0 the CD signal of the protein at this wavelength in the absence of the substrate analogue, Θ^{max} the maximum CD signal at substrate analogue saturation, and [AcP] the total concentration of the substrate analogue.

Spectroscopic Analysis of Cofactor Reaction Intermediates under Multiple-Turnover and Single-Turnover Conditions. To monitor changes in the protonation and/or ionization state of the cofactor aminopyrimidine part in the course of substrate turnover, UV−vis spectra were recorded in the 300−600 nm range after *Zm*PDC had been mixed with substrate pyruvate using a SX20 stopped-flow spectrophotometer equipped with diode array acquisition (Applied Photophysics).

Typically, ~10 mg/mL wild type or variant *Zm*PDC (corresponding to 164 μM active sites) in 50 mM MES (pH 6.0), 100 μM ThDP, and 1 mM Mg^{2+} was mixed with 20 mM pyruvate (in the same buffer) in a 1:1 mixing ratio at 30 °C using an optical path length of 10 mm. In the case of the wild-type enzyme, 200 spectra were recorded over a reaction time of 10.1 s (100 spectra in the first 100 ms; 100 spectra from 0.1 to 10.1 s). For the variants, a total of 200 spectra were collected at equal time intervals over 200 s. Spectra at steady state (wild type, 10 ms; variants, 10 s) were corrected for contributions of buffer, enzyme in the resting state (i.e., in the absence of pyruvate), and pyruvate. For spectroscopic analysis, pyruvate depletion is neglible because only ~100 μM pyruvate (wild type) or < 75 μM pyruvate (variants) is consumed after reaction for 10 ms or 10 s, respectively. This concentration change translates into a Δabsorbance of only ~0.002 at 320 nm, where pyruvate exhibits an n → π^* transition (ε = 20 M^{-1} s^{-1}).

In addition, single-turnover experiments were conducted in which 5 mg/mL protein (82 μM active sites) was mixed with an equimolar concentration of pyruvate in a 1:1 mixing ratio at 30 °C using the same buffer described above. Transients were recorded at specific wavelengths for each protein based on the band signature observed in the rapid-scan experiments.

Analysis of the Intermediate Distribution at Steady State and H−D Exchange Kinetics at C2 of ThDP by ^{1}H NMR after Acid Quench Isolation. To estimate unimolecular net rate constants of elementary catalytic steps (see Figure 1), the quantitative distribution of covalent reaction intermediates (LThDP and HEThDP) and of C2-unsubstituted ThDP under steady-state turnover conditions was analyzed by one-dimensional (1D) ^{1}H NMR spectroscopy after acid quench isolation as detailed in ref *3*.

In a typical experiment, 15 mg/mL *Zm*PDC in 50 mM potassium phosphate buffer (pH 6.0) was reacted with 100 mM sodium pyruvate (in the same buffer as protein) in a 1:1 mixing ratio (200 μL each) using a thermostated chemical quench-flow apparatus (RQF-3, Kintek Corp., Austin, TX). After a defined reaction time, ensuring that the steady state was established, the reaction was stopped (35 ms for the wild type and 60 s for the variants) by addition of an acidic quench solution [12.5% (w/v) trichloroacetic acid and 1 M DCl in D_2O]. Denatured protein was discarded after centrifugation. The clear supernatant containing pyruvate, products (acetaldehyde, acetoin, and acetate), and reaction intermediates in buffer was filtered (0.45 μm pore size) and further analyzed by 1D ^{1}H NMR spectroscopy at 300 K (Bruker Avance 400 NMR spectrometer). In the case of variant Glu473Gln, the experiments were also conducted at a protein concentration of 60 mg/mL to allow detection of low-population intermediates.

For the assignment and quantitative analysis of ThDP and covalent ThDP adducts, the C6′-H singlets of ThDP (8.01 ppm), LThDP (7.27 ppm), and HEThDP (7.33 ppm) were used.

The net rate constants of carbonyl addition of enzyme-bound pyruvate to ThDP [k'_2 (see Figure 1)], decarboxylation of LThDP (k'_3), and acetaldehyde liberation (k'_4) were estimated on the basis of the relative concentrations of the intermediates. It must be noted that the chemical quench−NMR method does not allow discrimination between HEThDP and its carbanion/enamine form because the latter will be instantaneously protonated in the course of acid quench isolation. Therefore, k'_4 is a composite rate constant and reflects both protonation of the carbanion/enamine intermediate (step 4a in Figure 1) and liberation of acetaldehyde (step 4b):

$$\frac{1}{k'_4} = \frac{1}{k'_{4a}} + \frac{1}{k'_{4b}} \tag{4}$$

Because formation of the reactive cofactor ylide form (k_0 in Figure 1) was shown previously not to be rate-limiting for *Zm*PDC catalysis (*22*), k_{cat} relates to the forward net rate constants at saturating substrate concentrations (substrate binding is not rate-determining under these conditions) as follows:

$$\frac{1}{k_{cat}} = \frac{1}{k'_2} + \frac{1}{k'_3} + \frac{1}{k'_4} \tag{5}$$

At steady state and [S] ≫ K_M, providing that the formation and decomposition of all reaction intermediates are balanced, i.e., d[intermediate]/dt ~ 0, the relative intermediate concentrations can be directly correlated with the unimolecular net rate constants of their interconversion.

$$\frac{[\text{E}-\text{LThDP}]}{[\text{E}-\text{ThDP}]} = \frac{k'_2}{k'_3} = a \tag{6}$$

$$\frac{[\text{E}-\text{HEThDP}]}{[\text{E}-\text{LThDP}]} = \frac{k'_3}{k'_4} = b \tag{7}$$

The fraction of isolated cofactor as C2-unsubstituted ThDP was corrected for fractional saturation of the enzyme with substrate according to the Michaelis−Menten equation. Using the experimentally determined steady-state intermediate distribution, k_{cat}, and eqs 5−7, the forward rate constants of single steps can be derived as follows:

$$k'_2 = k_{cat}(1 + a + ab) \tag{8}$$

$$k'_3 = k_{cat}\frac{1 + a + ab}{a} \tag{9}$$

$$k'_4 = k_{cat}\frac{1 + a + ab}{ab} \tag{10}$$

The deprotonation rate constant of enzyme-bound ThDP in the Glu473Gln variant was determined using an H−D exchange technique as described in ref *22*.

Protein Crystallization, Data Collection, and Structure Determination of Predecarboxylation Intermediate LThDP Trapped in ZmPDC Variant Glu473Asp. *Zm*PDC variant Glu473Asp was adjusted to a protein concentration of 5 mg/mL in 10 mM citrate buffer (pH 6.0) supplemented with 1 mM ThDP and 1 mM $MgSO_4$ and subsequently crystallized using the hanging vapor drop diffusion method against a reservoir solution of 100 mM MES buffer (pH 6.0), 1 mM ThDP, 5 mM $MgSO_4$, and 20−24% (w/v) polyethylene glycol 1500 as the precipitant. We deliberately omitted dithioerythritol from the crystallization mixture as reported in the published procedure (*10*) because we wished to minimize redox reactions and eventual destruction of the cofactor in the course of crystallization and data acquisition (the thiazolium portion of ThDP was found to be destroyed in the X-ray structure of wild-type *Zm*PDC). Crystals were grown at room temperature after mixing 2 μL of protein solution (5 mg/mL) with 2 μL of reservoir solution. Within 2 weeks, large but thin

platelike crystals of variant Glu473Asp with similar dimensions as previously reported were obtained. In view of the high occupancy of the LThDP intermediate in the Glu473Asp variant (>90%) in the liquid state (see the NMR studies in Results), we attempted to trap this intermediate in the crystalline state. Therefore, we soaked crystals of the Glu473Asp variant with 100 mM sodium pyruvate in the reservoir solution that was further supplemented with 20% (v/v) glycerol for approximately 5 min followed by flash-cooling of the crystals in liquid nitrogen. Initial processing of data sets collected in-house indeed revealed the LThDP intermediate to be formed in one crystal that diffracted up to a resolution of ~2.6 Å (most crystals tested exhibited a high mosaicity and were not suitable for X-ray structural analysis).

An X-ray data set of *Zm*PDC variant Glu473Asp in complex with predecarboxylation intermediate LThDP was then collected from a single crystal under cryoconditions (in a 100 K nitrogen stream) at BESSY beamline 14.2 (Berlin, Germany) using a 165 mm single-chip CCD detector from MARRESEACH (SX-165). A total of 675 images were collected over an angular range of 270° with a ϕ slicing of 0.4°. The diffraction data extended to a resolution of 1.98 Å. Initial processing of the entire data set in 80 image portions (1−80, 6−86, 11−91, etc.) using XDS revealed higher mosaicity and therefore larger amounts of overlapped reflections for some crystal orientations indicated also by high R_{merge} values (the highest R_{merge} values were observed for portions of images collected when the longest crystal dimension was parallel or close to parallel to the incoming X-ray beam). We therefore included only 360 images for the final data processing which resulted in a reflection file of reasonable completeness and redundancy which was used for refinement of the structure. Including more images resulted in much higher R_{merge} values of the data set and crystallographic *R*-factors calculated for the model. Oscillation images were integrated, merged, and scaled using XDS (*23*). The structure of *Zm*PDC variant Glu473Asp was determined by molecular replacement with PHASER using the structure of wild-type *Zm*PDC as a search model (PDB entry 1ZPD) (*24*). The variant crystallized in monoclinic space group *P*21 and comprises a functional tetramer in the asymmetric unit. Notably, the wild-type enzyme crystallized in primitive triclinic spacegroup *P*1 and also contains a tetramer in the asymmetric unit. Refinement of the structure was performed in CNS and PHENIX (both programs were using the same test set for calculating R_{free}), applying both overall anisotropic *B*-factor and bulk solvent corrections (*25*, *26*). Model rebuilding against difference as well as simulated annealing (SA) electron density omit maps has been conducted in COOT (*27*). The analysis of atomic displacements parameters of the refined structure revealed that the *B*-factors generally increase with the distance from the center of each domain forming one monomer (Pyr domain, R domain, PP domain), implying a rigid body libration of those domains. To model anisotropic displacements of these domains, the final refinement was conducted with PHENIX implementing 16 TLS groups (four groups per monomer: the three main domains and a flexible linker between the R and PP domains). The experimental as well as simulated annealing omit maps generated by CNS unambiguously showed the presence of Asp473 in the structure. In addition, simulated annealing omit maps were calculated for LThDP or for the pyruvate-derived lactyl moiety of LThDP. These maps clearly revealed that formation of the covalent bond between C2 of ThDP and the carbonyl carbon of pyruvate had taken place in the crystal as indicated by the strong continuous electron density between the two atoms. The crystallographic *B*-factors of the lactyl moiety of LThDP are comparable to those of the cofactor's thiazolium ring and thus suggest full occupancy of the intermediate. The final model of the Glu473Asp variant consisting of residues 2−566 of every monomer has been refined to a resolution of 1.99 Å, giving final R_{cryst} and R_{free} values of 0.1942 and 0.2456, respectively. For two monomers, a fragment of the linker between the R and PP domains could not be localized in electron density maps, suggesting local disorder of those regions (chain B, residues 351−355; chain D, residues 350−359). The model has good geometry as judged by MOLPROBITY (*28*), with 97.6% of the residues in the most favored regions of the Ramachandran plot and no residues marked as outliers. The final statistics of data collection and refinement are detailed in Table 1. Crystallographic figures were prepared with Pymol (DeLano Scientific, San Carlos, CA).

Table 1: Crystallographic Statistics for Variant Glu473Asp in a Complex with LThDP

Data Collection[a]	
wavelength (Å)	0.91841
space group	*P*2(1)
cell dimensions	a = 67.49 Å, b = 165.36 Å, c = 95.87 Å, β = 108.93°
resolution range (Å)	20.00−1.99 (2.10−1.99)
no. of observations	389596
no. of unique reflections	128527
completeness (%)	93.2 (83.3)
$\langle I/\sigma(I)\rangle$	16.6 (5.8)
R_{merge}[b] (%)	4.9 (17.9)
redundancy	3.03 (2.47)
B-factor from the Wilson plot (Å^2)	22.7
Refinement	
resolution range (Å)	19.58−1.99
no. of reflections (working/test)	128524/6426
R_{cryst},[c] R_{free}[d] (%)	19.4/24.6
mean *B*-factor (Å^2)	26.4
B-factor of the cofactor (Å^2)	26.1/26.2/30.4/25.4
no. of non-hydrogen atoms	18378
no. of water molecules	1256
rmsd for bond lengths (Å)	0.004
rmsd for bond angles (deg)	0.924
Ramachandran analysis (%)	
most favored	97.6
allowed	2.4

[a]Values in parentheses correspond to those for the highest-resolution shell. [b]$R_{merge} = \sum|I - \langle I\rangle|/\sum\langle I\rangle$. [c]$R_{cryst} = \sum||F_{obs}| - |F_{calc}||/\sum|F_{obs}|$. [d]$R_{free}$ is calculated as R_{cryst} but for a test set comprising reflections not used in the refinement (5.0%).

Density Functional Theory Studies on the Decarboxylation of LThDP. The reaction coordinates for the decarboxylation reaction of LThDP in different conformations were investigated by the density functional theory (DFT) method at the B3LYP/6-31G(d) level using GAUSSIAN03 (*29*). Recent DFT studies on thiamin models including more sophisticated basis sets have indicated that the 6-31G(d) standard is sufficient for a reliable analysis of such systems (*30*).

The aim of our studies here was to compare the reaction barriers for LThDP decarboxylation with either a perpendicular "maximum overlap" orientation of the scissile C2α−C(carboxylate) bond as previously observed for related tetrahedral substrate−ThDP adducts in other ThDP enzymes or a twisted (nonperpendicular) orientation of this bond as experimentally determined here

Table 2: Steady-State Kinetic Constants of Wild-Type *Zm*PDC and Its Variants[a]

	wild type	Glu473Asp	Glu473Gln
k_{cat} (s^{-1}	150 ± 5 (100%)	0.10 ± 0.003 (0.06%)	0.15 ± 0.004 (0.1%)
K_M (mM)	0.31 ± 0.03	0.15 ± 0.03	0.40 ± 0.05
k_{cat}/K_M (M^{-1} s^{-1})	4.84×10^5 (100%)	6.66×10^2 (0.14%)	3.75×10^2 (0.08%)
pK_a (k_{cat}/K_M)	6.23 ± 0.07[b]	6.28 ± 0.06	6.72 ± 0.02[b]
pK_a (k_{cat})	NA[c]	NA[c]	NA[c]

[a]Standard activity measurements were taken at 30 °C in 50 mM MES buffer (pH 6.0) containing 1 mM $MgSO_4$ and 100 μM ThDP. [b]From ref *20*. [c]Not applicable (k_{cat} not dependent on pH).

for LThDP in *Zm*PDC variant Glu473Asp. Because the decarboxylation of LThDP is severely impaired in the isofunctional variant (3−4 orders of magnitude slower than in wild-type *Zm*PDC), it is tempting to speculate that the decarboxylation is stereoelectronically affected.

The structural and functional characterization of ThDP enzymes provided clear evidence that the cofactor diphosphate moiety is required to provide tight binding to the target enzyme but is not involved in catalysis. Therefore, we have restricted our model calculations to the corresponding 2-lactylthiamin systems to reduce the computational error.

We have modeled the influence of the apoenzyme environment in a straightforward way by fixing the cofactor in the experimentally observed V conformation (torsion angles $\Phi_T = 105°$ and $\Phi_P = -61°$) by constraints in the optimization procedure. Moreover, the alternative orientations of the lactyl moiety were simulated by constraints for the S1−C2−C2α−COO^- torsion angle with −91° and −114° for the perpendicular (modeled) and twisted forms (taken from the experimentally determined X-ray structure), respectively. Moreover, we considered both the 1′,4′-imino and 4′-amino forms of LThDP in our calculations to test the possible influence of the aminopyrimidine's tautomeric state on decarboxylation.

In all calculations of the decarboxylation reaction, the C2α−COO^- distances (150−330 pm) were increased in 10 pm increments. The computations were performed on the SMP cluster of the computational center of the Martin-Luther University Halle-Wittenberg.

RESULTS

Steady-State Kinetics. The steady-state kinetic constants of wild-type *Zm*PDC and its variants (Glu473Asp and Glu473Gln) are summarized in Table 2. Both an isofunctional substitution and an isosteric substitution of Glu473 with Asp or Gln almost completely abolish catalytic activity (data not shown). The two variants exhibit a residual activity of 0.1% (Glu473Gln) or 0.06% (Glu473Asp), highlighting the central role of Glu473 for catalytic activity. The K_M value for substrate pyruvate is virtually unchanged in Glu473Gln (0.40 ± 0.05 mM) compared to that of the wild-type enzyme (0.31 ± 0.03 mM), whereas it is 2-fold smaller in the case of Glu473Asp (0.15 ± 0.03). The k_{cat} values of all three proteins are independent of pH over a range from 5 to 8. However, in all cases studied, the K_M constant for pyruvate increases at alkaline pH. In previous studies (*20*), quantitative analysis of pH versus k_{cat}/K_M revealed a pK_a of 6.23 ± 0.07 for wild-type *Zm*PDC when considering a single ionizable group to account for the observed pH dependence. A similar value can be estimated for variant Glu473Asp (pK_a = 6.28 ± 0.06), whereas it is slightly increased for Glu473Gln (pK_a = 6.72 ± 0.02).

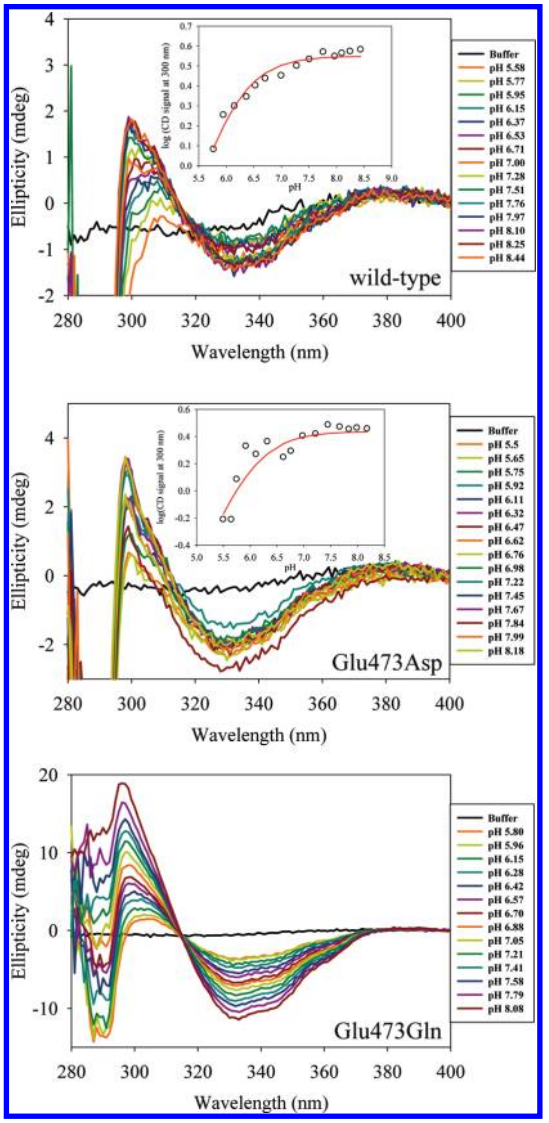

FIGURE 3: Near-UV CD spectra of 2 mg/mL (33 μM active sites) wild-type *Zm*PDC and its variants (Glu473Asp and Glu473Gln) in the resting state at different pH values. Experimental details are given in Materials and Methods. Insets shows the pH dependence of IP formation monitored at 300 nm. The pK_a was estimated using eq 2.

Analysis of Protonic and Tautomeric Equilibria of Enzyme-Bound ThDP by CD Spectroscopy. Near-UV CD spectra were recorded for wild-type *Zm*PDC and its two variants, Glu473Asp and Glu473Gln, at different pH values between 5.5 and 8.5.

The wild-type enzyme exhibits a negative band at ~320 nm and a positive band at ~300 nm indicating the coexistence of the amino form (AP, 320 nm) and the 1′,4′-imino tautomer (IP, 300 nm) of the cofactor aminopyrimidine in the resting state (Figure 3).

The amplitude of both signals increases with pH and reaches a limiting value at pH ~8. However, the change in signal intensity is more pronounced for the IP form, suggesting that it has a higher molar ellipticity than the AP band. Fitting the data to eq 2 yields a pK_a of 6.25 ± 0.08. The estimated pK_a pertains to the protonic equilibrium between the IP and AP tautomers and the aminopyrimidinium (APH^+) form, for which no CD signal assignment exists. The tautomeric IP ⇔ AP equilibrium appears to be pH-independent. Remarkably, the estimated pK_a of the cofactor [$APH^+ \leftrightarrow H^+ +$ (IP/AP)] in the resting state is identical to that determined for the pH dependence of k_{cat}/K_M under steady-state turnover conditions.

A similar outcome is observed for the Glu473Asp variant. The pK_a for the $APH^+ \leftrightarrow H^+ +$ (IP/AP) equilibrium was estimated to be 5.98 ± 0.12 and is close to the single-site pK_a (k_{cat}/K_M) under steady-state turnover conditions. The change in the AP signal is less pronounced than that of the IP form, analogous to the wild-type enzyme.

The results for variant Glu473Gln are somewhat different. Although the CD signal amplitudes of both the AP and IP forms are pH-dependent, they linearly increase with an increase in pH. As no signal saturation is observed, a pK_a cannot be reliably estimated. Moreover, the absolute CD signal intensity for both the IP and AP band is much higher than for wild-type and variant Glu473Asp, suggesting residue 473 critically determines the pK_a of the aminopyrimidine and the molar ellipticity of the ThDP signals.

Thermodynamic Analysis of Acetylphosphinate Binding by CD Spectroscopy. Acylphosphonates and acylphosphinates have turned out to be suitable substrate analogues for ThDP-dependent enzymes acting on 2-keto acids. When using such analogues, stable covalent predecarboxylation intermediate analogues are formed on the enzymes' active sites. In this way, substrate binding (encompassing formation of the substrate Michaelis complex and of the tetrahedral substrate−ThDP adduct) can be singled out for a detailed kinetic, thermodynamic, or even structural analysis (*14*). Binding of the pyruvate analogue methyl acetylphosphonate (MAP) did not result in a detectable change in the near-UV CD spectrum in any of the three *Zm*PDC proteins tested (data not shown). However, upon addition of the less bulky analogue acetylphosphinate (AcP) to wild-type *Zm*PDC, the signal intensity of both the IP band at ~300 nm and that of the AP band at ~320 nm increased in a concentration-dependent manner (Figure 4). Quantitative analysis according to eq 3 yielded similar dissociation constants (K_{app}) when using the IP band (450 ± 37 μM) and the AP band (317 ± 49 μM). It was previously suggested for related ThDP enzymes that the IP band indicates formation of the covalent AcP−ThDP adduct in half of the active sites, whereas the AP band is a reporter for the non-covalent substrate Michaelis complex (*4*). However, we consider such a half-of-the-sites mechanism unlikely in the case of *Zm*PDC because microscopic kinetic analysis of *Zm*PDC by NMR is not compatible with such a mechanism (*3*). Furthermore, our X-ray analysis indicates the presence of LThDP in all active sites of *Zm*PDC in the crystalline state (see Results), thus relegating an alternating sites mechanism to minor probability. Instead, we suggest that the IP and AP tautomers of predecarboxylation intermediates are both stabilized on the enzyme with an equilibrium constant close to unity.

Variant Glu473Asp binds acetylphosphinate with a comparable affinity and also displays a concentration-dependent increase in the magnitudes of both the IP and AP signals at 300 and

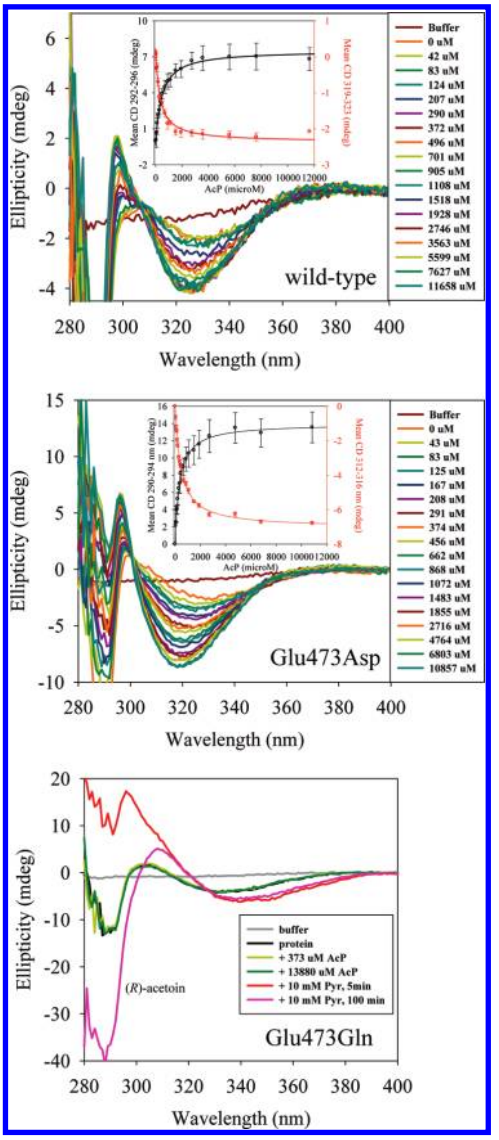

FIGURE 4: Near-UV CD spectra of 2 mg/mL (33 μM active sites) wild-type *Zm*PDC and its variants (Glu473Asp and Glu473Gln) at pH 6.0 titrated with the substrate analogue acetylphosphinate. Experimental details are given in Materials and Methods. Insets shows the concentration dependence of the IP and AP signals. Apparent dissociation constants were estimated using eq 3.

320 nm, respectively. The apparent dissociation constant of acetylphosphinate was estimated to be 366 ± 25 μM (IP signal) and 443 ± 22 μM (AP signal), indicating a minor change in K_{eq} between the IP and AP forms. Variant Glu473Gln was not able to bind the phosphinate analogue even when high concentrations were employed. Addition of the physiological substrate pyruvate, however, did lead to a change in the near-UV CD spectrum of the variant. After a 10 min reaction time, a negative CD band was formed at ~350 nm and a positive band at ~290−300 nm. While the former signal appears to pertain to a reaction intermediate in the AP form, the signal at 290 nm could originate either from an intermediate in the IP form or from products of off-pathway carboligation reactions. After prolonged reaction times (100 min), a negative CD signal pertaining to (*R*)-acetoin is observed. ^{1}H NMR analysis indeed confirms formation of acetoin apart from acetaldehyde and acetate, whereas acetolactate could not be detected (data not shown). Irrespective of this carboligation side reaction (product acetaldehyde reacts with $HEThDP^-$), the CD spectra clearly suggest the coexistence of the IP and AP forms at

Table 3: Microscopic Rate Constants for Elementary Steps in the Reactions of Wild-Type *Zm*PDC and Its Variants Glu473Asp and Glu473Gln[a]

	k_{cat} (s^{-1})	k_0 (s^{-1}) for cofactor activation	k'_2[b] (s^{-1}) for LThDP formation	k'_3[b] (s^{-1}) for decarboxylation	k'_4[b] (s^{-1}) for acetaldehyde liberation
wild-type *Zm*PDC	150	110 ± 19	2650	397	265
Glu473Asp *Zm*PDC	0.10 (1500)	104 ± 20 (~1)	0.60 (4400)	0.13 (3000)	1.2 (220)
Glu473Gln *Zm*PDC	0.15 (1000)	53 ± 20 (~2)	5.4 (500)	> 15 (nd)[c]	0.15 (1800)

[a]Rate constants of cofactor activation k_0 were estimated by kinetic analysis of H−D exchange at C2 of enzyme-bound ThDP at 5 °C, and net rate constants (see Figure 1) for formation of LThDP from bound pyruvate (k'_2), decarboxylation of LThDP (k'_3), and liberation of product acetaldehyde (k'_4) at saturating pyruvate concentrations of 50 mM were calculated using eqs 6−10, from k_{cat} and the distribution of ThDP-bound intermediates, determined by the acid quench−NMR method at 30 °C in 0.05 M potassium phosphate (pH 6.0). The major source of error in the analysis of the distribution of intermediates is the error in the integration of the individual signals of the intermediate species, and it is therefore dependent on the signal-to-noise ratio of the respective signals. Typically, the error varies between approximately 10 and 20%, the latter value being relevant for poorly resolved signals. Some of the data were reported in ref *3*. [b]Numbers in parentheses refer to the ratio of the rate constant calculated for wild-type *Zm*PDC divided by that of the respective variant (i.e., $k_{cat} = k_{cat}^{wt}/k_{cat}^{variant}$). [c]LThDP could not be detected by the acid quench−NMR analysis even at a concentration of 60 mg/mL. Therefore, a lower limit is calculated on the basis of a signal-to-noise ratio of 3 as a detection limit.

steady state in *Zm*PDC Glu473Gln. It is noteworthy that both bands exhibit a bathochromic shift of 10−20 nm relative to the corresponding forms in the resting state.

Analysis of the Intermediate Distribution at Steady State and H−D Exchange Kinetics at C2 of ThDP by ^{1}H NMR after Acid Quench Isolation. Our previous studies of cofactor activation in *Zm*PDC employing a H−D exchange technique had revealed that deprotonation of C2 of enzyme-bound ThDP cannot be kinetically resolved at 30 °C by rapid mixing because the reaction is completed within the dead time of mixing (~2 ms), thus giving a k_{obs} lower limit of > 600 s^{-1} (*22*). Kinetic analysis at 5 °C yielded a first-oder rate constant k_{obs} of ~110 s^{-1} for wild-type *Zm*PDC (Table 3). A similar rate constant was estimated for variant Glu473Asp (104 ± 20 s^{-1}). In variant Glu473Gln, cofactor activation is slightly impaired as evidenced by a 2-fold decreased rate constant of H−D exchange (53 ± 20 s^{-1}). In neither protein is cofactor activation (k_0 in Figure 1) rate-limiting for catalysis.

The quantitative distribution of reaction intermediates (C2-unsubstituted ThDP, LThDP, and HEThDP) in *Zm*PDC working at the steady state can be analyzed by 1D ^{1}H NMR spectroscopy after acid quench isolation. Our previous studies of wild-type *Zm*PDC showed that decarboxylation of LThDP (k'_3 ~ 397 s^{-1}) and acetaldehyde liberation (k'_4 ~ 265 s^{-1}) are both partially rate-determining for overall catalysis (k_{cat} = 150 s^{-1} at 30 °C) at saturating substrate concentrations (50 mM), whereas the unimolecular carbonyl addition of bound pyruvate to C2 of ThDP (k'_2 ~ 2650 s^{-1}) proceeds at least 1 order of magnitude faster (*3*). A different outcome is observed for the two variants (Figure 5). In Glu473Asp, the reaction stalls at the LThDP state under steady-state turnover conditions, indicating decarboxylation of this intermediate (k'_3 = 0.13 s^{-1}) is rate-determining for overall catalysis (k_{cat} = 0.1 s^{-1} at 30 °C). Thus, decarboxylation of LThDP in Glu473Asp proceeds 3000-fold slower than in the wild-type enzyme. Although not rate-limiting, both formation of LThDP and acetaldehyde liberation are also compromised by several orders of magnitude in the variant, pointing to a global role of Glu473 in *Zm*PDC catalysis. Contrary to the isofunctional substitution of Glu473 with Asp, an isosteric Glu → Gln substitution has no measurable effect on decarboxylation as no LThDP is detected at steady state even at a protein concentrations as high as 60 mg/mL for the chemical quench−NMR experiments. Instead, the variant accumulates HEThDP to almost full occupancy, implying acetaldehyde liberation to be severely impaired (k'_4 = 0.15 s^{-1}) when compared to the wild-type situation (k'_4 ~ 265 s^{-1}). Because the quench−NMR methodology does not permit discrimination between the carbanion/enamine intermediate and the C2α-protonated forms of HEThDP, at this point no distinction between which of the two HEThDP forms (carbanion/enamine or conjugate acid) is accumulated in the variant can be made.

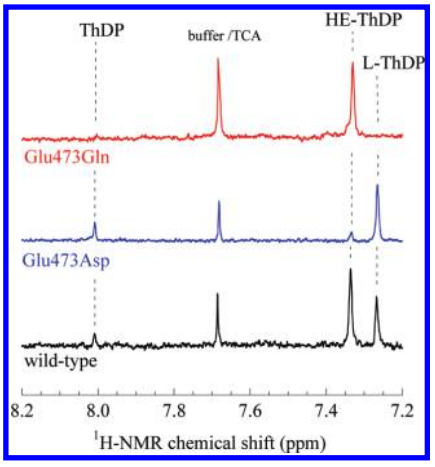

FIGURE 5: Steady-state intermediate distribution of reaction intermediates in the nonoxidative decarboxylation of pyruvate by wild-type *Zm*PDC and its variants (Glu473Asp and Glu473Gln) at substrate saturation (50 mM). The intermediates were isolated by acid quench after a reaction time of either 35 ms (wild type) or 60 s (variants) in 50 mM potassium phosphate buffer (pH 6.0) at 30 °C and analyzed by 1D ^{1}H NMR at pH 0.75 using the chemical shifts of the C6′-H singlets of C2-unsubstituted ThDP (8.01 ppm), HEThDP (7.33 ppm), and LThDP (7.27 ppm) for quantitation.

Spectroscopic Analysis of Cofactor Reaction Intermediates under Multiple-Turnover and Single-Turnover Conditions Using a Stopped-Flow Method. To analyze possible changes in the protonic and/or tautomeric states of enzyme-bound ThDP in the course of substrate turnover, time-resolved spectra were recorded after wild-type *Zm*PDC or its variants had been mixed with a saturating concentration of pyruvate (10 mM after mixing) at 30 °C. Difference spectra between the steady state (wild type at 10 ms and variants at 10 s) and resting state (prior to mixing) were calculated (Figure 6). In wild-type *Zm*PDC, the buildup of a spectroscopic band at ~310 nm accompanies the establishment of the steady state indicating the presence of reaction intermediates in the IP form. In variant Glu473Asp, which accumulates LThDP at the steady state, a similar absorbance band pertaining to the imino tautomer is formed upon mixing with pyruvate, although it is approximately 5-fold more intense than that of the wild type and further exhibits a slight

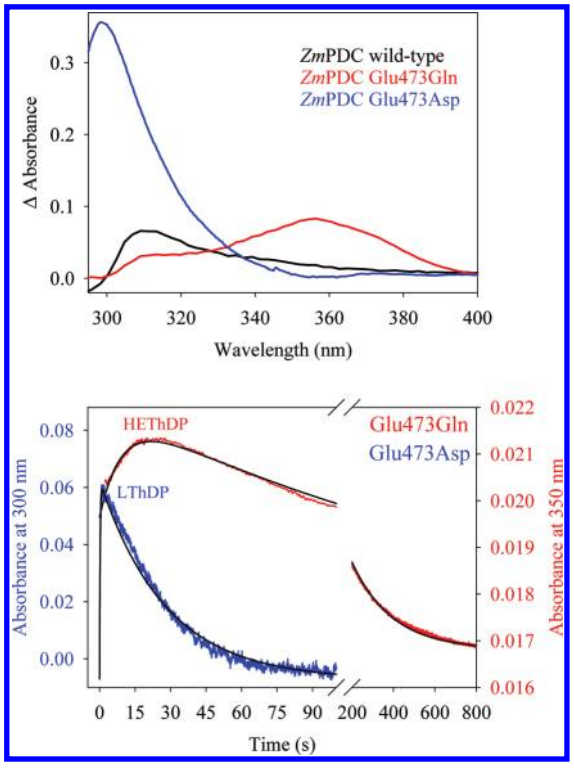

FIGURE 6: Spectroscopic detection of cofactor reaction intermediates on wild-type *Zm*PDC and variants (Glu473Asp and Glu473Gln). The top panel shows difference absorbance spectra between the steady state and the resting state. Enzyme (10 mg/mL) in 50 mM MES (pH 6.0), 100 μM ThDP, and 1 mM Mg^{2+} was mixed with either 20 mM pyruvate or buffer in a 1:1 mixing ratio at 30 °C. Absorbance spectra obtained after protein and buffer (resting state) had been mixed were subtracted from spectra at the steady state (10 ms for the wild type and 10 s for the variants) recorded after protein and substrate had been mixed. The bottom panel shows single-turnover kinetics for variants Glu473Asp and Glu473Gln. Stopped-flow transients were recorded at either 300 nm (Glu473Asp) or 350 nm (Glu473Gln) after 5 mg/mL enzyme (82 μM active sites) had been mixed with an equimolar concentration of pyruvate in a 1:1 mixing ratio at 30 °C using the same buffer described above. Transients were fitted to a double-exponential function and yielded (pseudo)-first-order rate constants for buildup and depletion of either LThDP (on Glu473Asp) or HEThDP carbanion/enamine (on Glu473Gln). Rate constants are given in the text.

hypsochromic shift. A totally different outcome is observed for the Glu473Gln variant, which gives rise to an absorbance increase at ~350−360 nm and to a lesser degree at ~310 nm paralleling the CD spectroscopic results (see Figure 4). Because our NMR-based intermediate analysis at the steady state revealed accumulation of HEThDP to full occupancy in this variant, the long-wavelength band at 350−360 nm should pertain to either the carbanion/enamine form of HEThDP or, alternatively, its conjugate acid (protonated at C2α). Previous studies of *Sc*PDC and other ThDP-dependent enzymes suggested tetrahedral ThDP intermediates such as HEThDP (C2α-protonated) to preferentially stabilize the IP form that exhibits CD and absorbance bands at 300−310 nm (*4*). In light of these precedents, we tentatively assign the long-wavelength band in Glu473Gln to the carbanion/enamine form of HEThDP. Because model studies of thiazolium-based enamines suggest these compounds have absorption bands at < 300 nm (*31*), the observed band in Glu473Gln presumably originates from an intramolecular charge-transfer complex between the aminopyrimidine (AP form, presumed donor) and the hydroxyethylidene−thiazolium moiety of HEThDP (presumed acceptor).

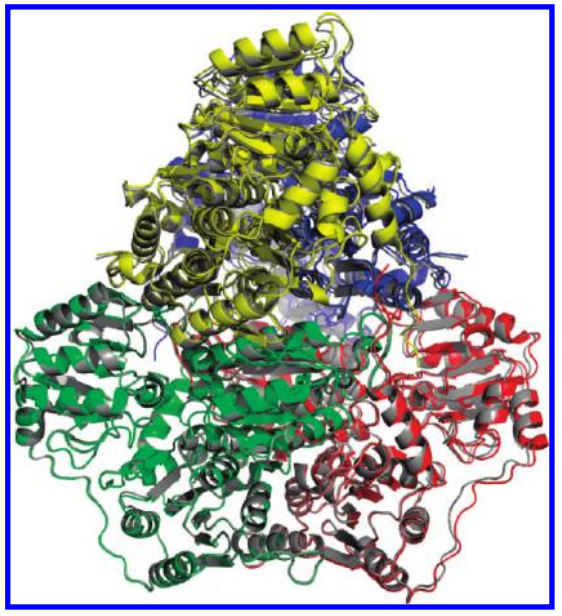

FIGURE 7: Superposition of wild-type *Zm*PDC and variant Glu473Asp tetramers in cartoon representation. The individual subunits of the wild-type protein are highlighted by a different color code, and the tetramer of the variant is colored gray.

To gather additional kinetic information about the lifetime of covalent intermediates, we conducted single-turnover experiments in which *Zm*PDC was reacted with an equimolar amount of pyruvate. Transients were recorded at 310 nm (wild type), 300 nm (Glu473Asp), and 350 nm (Glu473Gln) to selectively monitor the buildup and depletion of reaction intermediates relying on the signals of the different forms of the cofactor aminopyrimidine.

The reaction of wild-type *Zm*PDC and pyruvate could not be kinetically resolved because pyruvate was depleted within the dead time of the stopped-flow instrument (2 ms) (data not shown). However, the formation and decay of reaction intermediates could be analyzed in the two Glu473 variants using stopped-flow kinetics. In variant Glu473Asp, transient formation of LThDP was monitored at 300 nm where the IP form of this intermediate gives rise to an absorbance signal. The stopped-flow transient could be fitted to a double-exponential function. LThDP is formed with a pseudo-first-order rate constant of $3.78 \pm 0.02\ s^{-1}$ and decays with a first-order rate constant of $(3.46 \pm 0.01) \times 10^{-2}\ s^{-1}$. In variant Glu473Gln, the transient formation of the HEThDP carbanion/enamine intermediate was monitored at 350 nm where its AP form absorbs. Here, buildup of the intermediate takes place with a pseudo-first-order rate constant of $(1.09 \pm 0.01) \times 10^{-1}\ s^{-1}$, and it is depleted with a k of $(5.14 \pm 0.01) \times 10^{-3}\ s^{-1}$. Hence, substrate binding and processing until the LThDP (Glu473Asp) or HEThDP (Glu473Gln) state are severely impaired in the two variants, supporting the results of the NMR-based intermediate analysis at the steady state. Further, the rate constant of decarboxylation in the stopped-flow single-turnover experiments (~$0.04\ s^{-1}$) is very similar to that estimated by NMR analysis (~$0.1\ s^{-1}$). However, the lifetime of the HEThDP carbanion/enamine intermediate in variant Glu473Gln is markedly longer under single-turnover conditions than under steady-state turnover conditions.

X-ray Structure of LThDP Trapped in Variant Glu473Asp. The high occupancy of single intermediates in variants Glu473Asp (LThDP) and Glu473Gln (HEThDP carbanion/enamine) under

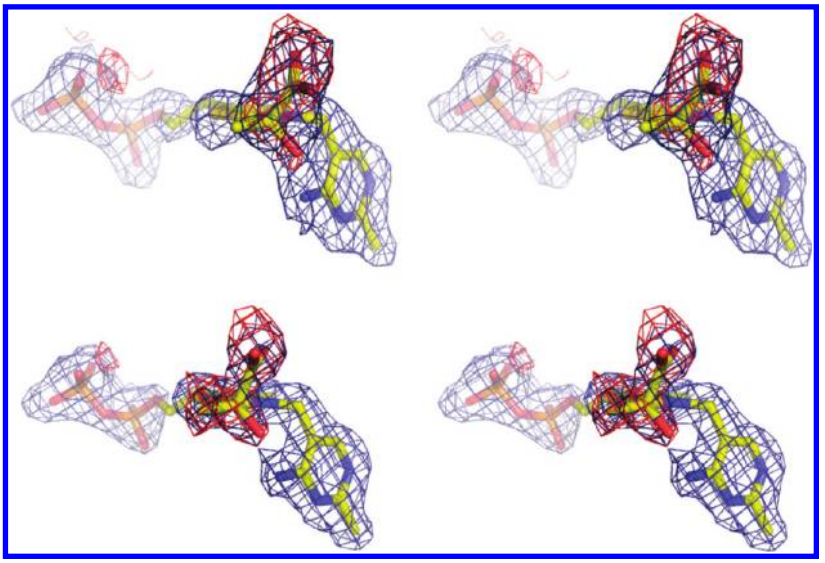

FIGURE 8: X-ray structure of predecarboxylation intermediate LThDP at the active center of *Zm*PDC variant Glu473Asp in stereoview, exemplified for two active sites. A $2F_o - F_c$ map of the final model (blue, contoured at 1σ) and a simulated annealing $F_o - F_c$ omit map (red, contoured at 3σ) are shown. For calculation of the simulated annealing omit maps, atoms of the lactyl moiety were omitted from the final model. Simulated annealing omit maps were calculated with CNS using a slow cooling protocol (1000 K start temperature, 25 K cooling per cycle, 0.004 ps time steps, and six steps per cycle) with torsion angle dynamics.

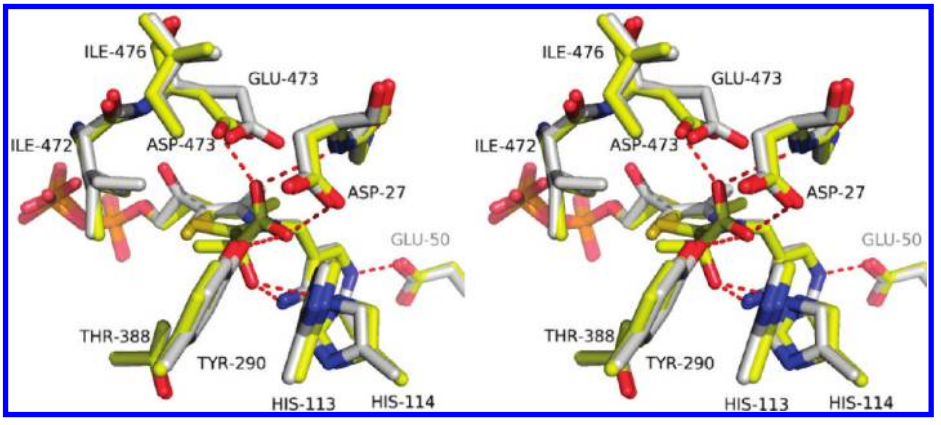

FIGURE 9: Superposition of the active site of wild-type *Zm*PDC in the resting state (gray) and variant Glu473Asp in complex with reaction intermediate LThDP (yellow). Hydrogen bonding interactions (< 3.3 Å contacts) are indicated by dotted lines.

steady-state turnover conditions renders possible a structural characterization of these intermediates in the enzyme-bound state by means of X-ray crystallography. Although crystals of both variants could be grown, only crystals of variant Glu473Asp were suitable for crystallographic analysis, while all crystals of the Gln variant did not diffract below 5 Å resolution. Even in the case of variant Glu473Asp, only one of 10 crystals diffracted below 3 Å resolution. After a single crystal of variant Glu473Asp had been soaked with pyruvate for a couple of minutes, it was subsequently flash-cooled in liquid nitrogen, and a data set was recorded at BESSY. The crystal structure of the variant in complex with reaction intermediate LThDP has been determined by molecular replacement phasing using the structure of wild-type *Zm*PDC as a search model (PDB entry 1ZPD) and refined to R_{cryst} and R_{free} values of 0.194 and 0.246, respectively, against data to 1.99 Å resolution. The variant crystallized in space group $P2_1$ with a tetramer in the crystallographic asymmetric unit. The structure of the variant is almost identical to that of the wild type (Figure 7); least-squares alignment of the two structures gave an rmsd of 0.32 Å for a monomer and 0.56 Å for the functional tetramer, corresponding to small shifts in the relative organization of domains, which form the intact subunits, and in the tetrameric assembly. Initial omit as well as simulated annealing omit maps indicated that the covalent predecarboxylation intermediate LThDP had been formed in all four active centers in the tetramer, arguing against the half-of-the-sites reactivity of *Zm*PDC (Figure 8). The electron density maps suggest the intermediate to be formed as the *S*-enantiomer in all active sites in analogy to the apparently conserved stereochemical course of substrate binding observed in other ThDP enzymes. The C2α atom of the intermediate is slightly out of the aromatic ring plane of the thiazolium portion (1−2°) even against opposing in-plane restraints in the refinement procedure, although the resolution precludes any definite statement about whether there is angular strain in the intermediate. However, a marked difference between LThDP in *Zm*PDC variant Glu473Asp and any other structurally characterized tetrahedral substrate−ThDP adduct relates to the orientation of the scissile C2α−C(carboxylate) bond. Whereas the scissile bonds of tetrahedral intermediates in all precedents were almost perfectly directed perpendicular to the thiazolium ring plane in a so-called "maximum overlap conformation" (*12*, *32*−*36*), the corresponding bond of LThDP in variant Glu473Asp deviates

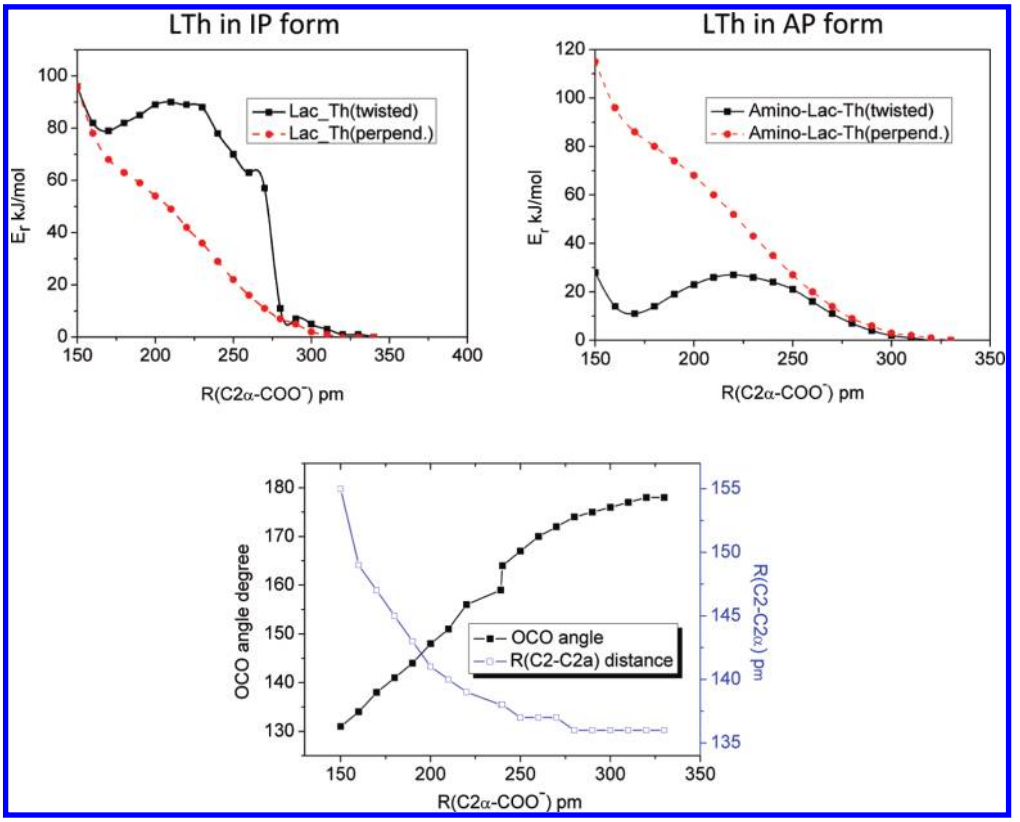

FIGURE 10: DFT studies of decarboxylation of lactylthiamin models. The top panels show the reaction coordinate for decarboxylation of lactylthiamin with either a perpendicular (S1−C2−C2α−COO^- torsion angle of −91°) or nonperpendicular orientation (S1−C2−C2α−COO^- torsion angle of −114° as experimentally observed in variant Glu473Asp) of the C2α−C(carboxylate) bond relative to the thiazolium ring plane. Reaction coordinates were calculated for both the IP and AP forms of the cofactor aminopyrimidine portion. The cofactor was fixed in the V conformation (torsion angles Φ_T = 105° and Φ_P = −61°) by constraints in the optimization procedure. The bottom panel shows the dependence of the O−C−O angle (carboxylate group of LThDP) and of the C2−C2α bond length on the interatomic distance between C2α and C(carboxylate).

from this optimal perpendicular orientation by ∼20−30°, with small differences in the four active sites (Figure 8).

The geometry of all active site residues is virtually unchanged in the variant compared to that in the wild-type structure, indicating that neither the substitution nor formation of the reaction intermediate is accompanied by a structural reorganization of the active site (Figure 9). The substituted Asp473 residue adopts an extended conformation such that one oxygen atom of the β-carboxyl(ate) occupies a position similar to that of the corresponding oxygen of the γ-carboxyl(ate) of Glu473 in wild-type *Zm*PDC, whereas the other O-carboxyl(ate) atom is displaced by approximately 1.5 Å. As a consequence of the twisted (nonperpendicular) conformation of the C2α−C(carboxylate) bond, the carboxyl(ate) groups of LThDP and of side chain 473 do not pair up as presumably realized in the wild-type enzyme (compare Figure 2A). The carboxylate of LThDP in variant Glu473Asp forms multiple hydrogen bonds with active site side chains and the main chain. One carboxylate oxygen interacts with Asp473 and the backbone amide of Asp27, and the second O atom is held in place by hydrogen bonding interactions with Tyr290 and Asp27.

Density Functional Theory Studies of the Decarboxylation of LThDP. The reaction coordinate for decarboxylation of LThDP to the HEThDP carbanion/enamine intermediate and CO_2 was analyzed by DFT studies. Our CD spectroscopic experiments using AcP as a substrate analogue had revealed that predecarboxylation intermediates are stabilized both in the IP form and in the AP form of the cofactor aminopyrimidine. Therefore, the decarboxylation of both tautomers of LThDP was studied. In this context, we have only considered the cofactor intermediate without including neighboring amino acid side chains. Because the scissile C2α−C(carboxylate) bond of LThDP in the *Zm*PDC variant is not oriented perpendicular to the thiazolium ring plane as commonly observed in ThDP intermediates, we analyzed both the experimentally observed twisted conformation and the perpendicular orientation, which is expected to be formed in the wild-type enzyme.

The DFT analysis clearly reveals (Figure 10) that decarboxylation of lactylthiamin proceeds barrierless, when the C2α−C(carboxylate) bond is oriented perpendicular to the thiazolium ring. This finding holds true for both the IP form and the AP form of LThDP. In the twisted conformation, however, an activation barrier for decarboxylation is detectable that is slightly different for the IP (10 kJ/mol) and AP (18 kJ/mol) forms. These findings demonstrate that decarboxylation of LThDP is indeed stereoelectronically affected and thus supports the proposed maximum-overlap mechanism of decarboxylation. The energies of the perpendicular and twisted forms of LThDP were similar when the IP form was considered (Figure 10). In contrast, the twisted conformation was found to be more than 80 kJ/mol more stable than the perpendicular one in the case of the AP form (Figure 10). Irrespective of which cofactor form (AP or IP) is subjected to the DFT analysis, decarboxylation is an exergonic process. In our model studies, a planar enamine-type HEThDP intermediate is formed upon decarboxylation with a double bond between C2 and C2α (Figure 10, bottom). It is questionable,

however, whether such a low-energy intermediate is being formed on the enzyme. Previous X-ray crystallographic studies on several ThDP enzymes revealed that the C2α atom of postelimination intermediates is out of the aromatic ring plane of the thiazolium nucleus already, indicating that ThDP enzymes might avoid the formation of (overly) stable intermediates (*13*).

DISCUSSION

PDC belongs to a family of enzymes that utilize ThDP as the biologically active form of vitamin B_1 as a bioorganic cofactor. Despite a remarkably conserved cofactor binding mode, ThDP enzymes catalyze a wide variety of different multistep reactions even though the reaction patterns are similar or analogous. In recent years, structural and functional evidence that suggests that the stereochemical course of substrate binding and processing is also a conserved feature in this enzyme family has been described (*14*). ThDP enzymes have apparently evolved a common and stereospecific three-center binding mode, according to which (i) the substrate leaving group (CO_2^- in the case of pyruvate), (ii) the substrate carbonyl, and (iii) the substrate substituent (CH_3 in the case of pyruvate) are each accommodated in shape-complementary pockets with specific interactions. In all precedents reported so far, the absolute configuration of the intermediate C2α stereocenter is identical, with the *S*-enantiomer of LThDP trapped in POX serving as a prototype (*14*). The scissile bond of tetrahedral substrate−ThDP adducts is directed perpendicular relative to the thiazolium ring plane such that the leaving group is positioned at the *re*-side of C2. The substrate carbonyl points toward the 4′-amino group of the aminopyrimidine, and consistent with these structural observations, functional analysis implicates the aminopyrimidine to act as an intramolecular acid/base catalyst in the course of carbonyl addition of substrate (protonation of the carbonyl O) and substrate liberation (deprotonation of C2α-OH) involving delicately balanced protonic and tautomeric equilibria among the three different forms of the cofactor aminopyrimidine (AP, APH^+, and IP).

Here, we have analyzed the functional role of residue Glu473 for *Zm*PDC catalysis in molecular detail. This side chain is located directly above the *re*-face of the thiazolium ring of ThDP and has been suggested to be part of the carboxylate pocket, to which the pyruvate-derived carboxylate of the LThDP intermediate will bind (Figure 2) (*3*). In our studies, we have considered single-site variants with either isofunctional (Glu → Asp) or isosteric (Glu → Gln) substitution to discriminate between effects related to size or chemical function. Steady-state kinetic analysis revealed that either substitution is detrimental for catalysis as evidenced by residual activities of 0.1% (Glu473Gln) or 0.06% (Glu473Asp). The K_M value for pyruvate is barely affected in both variants (Table 2).

Glu473 Modulates the Intrinsic Protonic and Tautomeric Equilibria of the Cofactor. The catalytic activity of *Zm*PDC is affected by pH. However, k_{cat} is virtually unchanged between pH 5 and 8, and the observed effect almost entirely results from changes in k_{cat}/K_M, i.e., substrate binding. The dependence of k_{cat}/K_M on pH can be described well by a model taking into account a single ionizable group. The pK_a of this group was estimated to be 6.23 ± 0.07 in wild-type *Zm*PDC, and a similar value was determined here for variant Glu473Asp (6.28 ± 0.06); on the other hand, the pK_a is slightly increased in variant Glu473Gln (6.72 ± 0.02). In accordance with a previous suggestion (*20*), CD spectroscopic analysis of the protonic and tautomeric equilibria of the bound cofactor in the resting state of *Zm*PDC identifies this "ionizable group" as the cofactor aminopyrimidine. In wild-type *Zm*PDC, the near-UV CD spectra suggest the coexistence of the AP (negative band at ~320 nm) and IP forms (positive band at ~300 nm) in the enzyme's resting state. At the expense of APH^+, the magnitude of the signal of both forms increases with pH and reaches a plateau at pH ~8. However, the molar ellipticity of IP is markedly higher than that of AP. Our results indicate that the IP and AP forms are in a pH-independent equilibrium, whereas both tautomers are in a pH-dependent equilibrium with the APH^+ form. This observation is consistent with results obtained for other ThDP enzymes, which revealed that the IP/AP tautomer couple is in a pH-dependent equilibrium with APH^+ (*37*). The pK_a for the $APH^+ \leftrightarrow H^+ +$ IP/AP equilibrium in *Zm*PDC was estimated to be 6.25 ± 0.08 and thus matches the pK_a estimated from the pH dependence of k_{cat}/K_M under steady-state turnover conditions. A similar coincidence of the two pK_a values is observed for variant Glu473Asp, whereas the intrinsic cofactor equilibria are clearly perturbed in variant Glu473Gln, suggesting that an acidic residue is required at position 473 for a fully functional aminopyrimidine. In line with this suggestion, both wild-type *Zm*PDC and variant Glu473Asp bind the substrate analogue acetylphosphinate with similar affinity, whereas variant Glu473Gln fails to bind the analogue. As also observed for the resting state, the predecarboxylation intermediate (the covalent acetylphosphinate−ThDP adduct) stabilizes the IP and AP forms. This indicates a different protonation-state requirement for *Zm*PDC catalysis compared to other ThDP enzymes, where predecarboxylation intermediates were shown to be almost exclusively stabilized in the IP form (*4*). We cannot ultimately exclude the possibility that the IP and AP bands report formation of different catalytic states as suggested for other ThDP enzymes in an alternating sites mechanism (*4*); however, both microscopic kinetic analysis in the liquid state and structural analysis by X-ray crystallography are inconsistent with half-of-the-sites reactivity in *Zm*PDC.

Although our CD spectroscopic studies could identify the cofactor aminopyrimidine as the ionizing group responsible for the pH dependence of k_{cat}/K_M, it is still unclear which catalytic step is reflected by this dependence. The cofactor aminopyrimidine is supposed to be involved as an acid/base catalyst in cofactor activation (step 0 in Figure 1, deprotonation of C2 by IP), carbonyl addition of bound pyruvate to ThDP (step 2, protonation of carbonyl O by APH^+), and elimination of acetaldehyde (step 4b, deprotonation of C2α-OH by IP). As k_{cat} is not affected by pH, cofactor activation and product liberation can be excluded to account for the observed pH dependence. Hence, it is highly likely that protonation of C2α-O^- (the alkoxidic form of LThDP) by APH^+ accounts for the pH dependence of k_{cat}/K_M.

Cofactor activation was found not to be rate-limiting in any of the three proteins. The observed first-order rate constants of H−D exchange at C2 of ThDP are very similar for the wild type and variant Glu473Asp (Table 3), which is consistent with the observation of similar intrinsic equilibria of the cofactor. Although these equilibria are apparently thermodynamically perturbed in variant Glu473Gln, the rate constant of H−D exchange is only 2-fold smaller than in the wild-type enzyme.

Intermediate Analysis by Optical and NMR Spectroscopy Suggests Multiple Roles of Glu473 for Binding and Catalysis. The quantitative distribution of reaction intermediates in *Zm*PDC turning over pyruvate was analyzed by 1D

^{1}H NMR spectroscopy after acid quench isolation. In wild-type *Zm*PDC, there is significant accumulation of both LThDP and HEThDP at the steady state, indicating that both decarboxylation of LThDP and liberation of acetaldehyde from HEThDP are partially rate-determining for overall catalysis (Figure 5). The difference absorbance spectrum between the steady state and resting state shows a slight increase in the intensity of the IP band at 310 nm, whereas no change is detectable at longer wavelengths, consistent with the predominant formation of tetrahedral intermediates (Figure 6). In Glu473Asp, the reaction stalls at the predecarboxylation LThDP state, demonstrating that the variant is deficient in catalyzing decarboxylation of this intermediate (Figure 5). Kinetic analysis shows that decarboxylation of LThDP in Glu473Asp ($k'_3 \sim 0.13\ s^{-1}$) is 3000-fold slower than in the wild-type enzyme ($k'_3 \sim 400\ s^{-1}$), which translates into an increase in the activation barrier of ~20 kJ/mol (Table 3). The UV−vis difference absorbance spectrum suggests LThDP to be exclusively stabilized in the IP form. In contrast, the postdecarboxylation intermediate HEThDP$^-$ is accumulated to almost full occupancy at steady state in variant Glu473Gln, implying this variant to be defective in product liberation (step 4a and/or step 4b in Figure 2). The microscopic net rate constant of acetaldehyde liberation in the variant ($k'_4 \sim 0.15\ s^{-1}$) is 2000-fold smaller than that of the wild-type enzyme ($k'_4 \sim 265\ s^{-1}$). The stopped-flow rapid-scan experiments revealed that the establishment of the steady state is accompanied by the buildup of a prominent UV−vis band centered around 350−360 nm (Figure 6). A negative band in this spectral region can also be detected by near-UV CD spectroscopy (Figure 4). The signature of the CD band suggests it to pertain to the AP form of HEThDP (carbanion/enamine or conjugate acid). Because the cofactor IP and AP forms in the resting state and in the tetrahedral predecarboxylation state exhibit bands at ~300 and ~320 nm, this long-wavelength band in Glu473Gln is unlikely to pertain to a tetrahedral intermediate, i.e., the C2α-protonated form of HEThDP. Conversely, we suggest this band pertains to the AP form of the HEThDP carbanion/enamine intermediate. Provided this tentative assignment is correct, this would have immediate implications for defining the role of Glu473 in *Zm*PDC catalysis. Because the Glu473Gln variant is deficient in protonation of the HEThDP carbanion/enamine intermediate, Glu473 can be identified as the acid/base catalyst that protonates the carbanion/enamine intermediate. The band assignment further invites us to revisit the data obtained for wild-type *Zm*PDC and Glu473Asp. These two proteins accumulate HEThDP at the steady state as revealed by NMR, but there is no evidence of the appearance of the long-wavelength band at 360 nm assigned to the HEThDP carbanion/enamine intermediate. Hence, the HEThDP carbanion/enamine intermediate must be very short-lived in the two proteins. The detailed kinetic analysis of variant Glu473Gln does not indicate that decarboxylation of LThDP is affected in the variant. This finding is not consistent with a mechanism that would invoke electrostatic stress between residue 473 and the carboxylate of LThDP as a driving force for decarboxylation. Such a mechanism has been proposed for other decarboxylating enzymes, e.g., OMDCase (*38*). Also, because variant Glu473Gln is apparently defective in protonating the carbanion/enamine intermediate but still efficiently catalyzes decarboxylation of LThDP, it appears unlikely that carbanion protonation by Glu473 drives decarboxylation of LThDP by preventing an internal return of CO_2 as previously shown in model reactions (*39*, *40*).

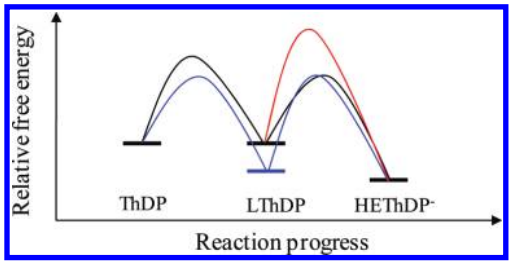

FIGURE 11: Simplified scheme of the free energy as a function of reaction progress in *Zm*PDC catalysis until the stage of the HEThDP carbanion/enamine intermediate (black). In addition, different scenarios that could account for a higher activation barrier of decarboxylation, including reactant-state stabilization of the predecarboxylation state (blue) and transition-state destabilization of the decarboxylation transition state (red), are shown.

Besides the functional importance of Glu473 for decarboxylation of LThDP and protonation of the incipient carbanion/enamine intermediate, our NMR and single-turnover stopped-flow kinetics further suggest a crucial role of this side chain in substrate binding. While pyruvate is completely converted to acetaldehyde by wild-type *Zm*PDC within the dead time of the stopped-flow instrument (1−2 ms), substrate binding is clearly affected in the two Glu473 variants. Here, substrate binding and processing until the LThDP (Glu473Asp) or the HEThDP carbanion/enamine intermediate (Glu473Gln) state takes place on a time scale of seconds (Figure 6).

X-ray Structural Analysis of Reaction Intermediates and DFT Analysis Suggest Decarboxylation of LThDP Is Stereoelectronically Controlled or Affected. The side chain of Glu473 is located in the proximity of the thiazolium part of ThDP and thus suitably positioned to interact with reaction intermediates (Figure 2). While its catalytic role as a general acid is conceivable, it is less clear how decarboxylation of LThDP is facilitated by this residue when electrostatic stress or a chemical coupling of decarboxylation and carbanion protonation as the potential driving force can be relegated to minor probability (see above). In principle, a higher activation barrier of the decarboxylation reaction could result from a stronger reactant-state stabilization of the predecarboxylation intermediate and/or from a transition-state destabilization state relative to the wild-type situation (Figure 11). It is important to note in this regard that decarboxylation of LThDP in the isofunctional Glu473Asp variant is dramatically slowed (3000-fold) compared to that in the wild-type enzyme, corresponding to a $\Delta\Delta G^{\ddagger}$ of 20 kJ/mol, although the intrinsic cofactor equilibria in the variant are not perturbed and substrate analogue acetylphosphinate is bound with virtually the same affinity as in the wild type. Consequently, a stronger thermodynamic stabilization of the predecarboxylation intermediate state, i.e., reactant-state stabilization, cannot account for the higher activation barrier of decarboxylation. To gather structural information about the long-lived LThDP intermediate in Glu473Asp, we determined the X-ray structure of the variant in complex with LThDP at a resolution of 1.99 Å. Because a reference structure of wild-type *Zm*PDC with bound LThDP could not be observed because LThDP is too short-lived and does not accumulate to a measurable occupancy, we must rely on structures of tetrahedral substrate/ThDP intermediates in other enzymes (*12*, *32*−*36*). The LThDP intermediate in Glu473Asp is formed as the *S*-enantiomer and is held in place by numerous hydrogen bonding interactions (Figure 9). Although the absolute configuration of the C2α stereocenter is

identical to that of related intermediates in other ThDP enzymes (*12*, *32*−*36*), LThDP in variant Glu473Asp exhibits a unique structural feature. The scissile C2α−C(carboxylate) bond is not directed perpendicular to the thiazolium ring plane but rather deviates from this maximum overlap orientation by 25−30°. In all precedents, leaving groups in ThDP intermediates were found to be oriented perpendicular to the thiazolium.

To test whether the structurally observed, nonperpendicular orientation of the carboxylate leaving group of LThDP in Glu473Asp could account for the impaired decarboxylation in this variant, we have conducted DFT studies on the decarboxylation reaction in lactylthiamin models. This analysis revealed that decarboxylation of (*S*)-lactylthiamin proceeds in a barrierless fashion when the carboxylate leaving group is oriented perpendicular, consistent with experiments with the wild-type enzyme. However, a substantial activation barrier of 10 kJ/mol (lactylthiamin in the IP form) or 18 kJ/mol (lactylthiamin in the AP form) exists for the twisted (nonperpendicular) conformation as experimentally observed in variant Glu473Asp. In conclusion, there is a strong stereoelectronic effect on the transition state of decarboxylation. The estimated differences in the activation barriers could account for the determined kinetic effects ($\Delta\Delta G^{\ddagger}$ of 20 kJ/mol for LThDP decarboxylation in Glu473Asp relative to that of the wild type). We have to admit, however, that the DFT analysis of lactylthiamin models in the absence of protein functional groups may have limitations. Our NMR studies on *Zm*PDC had revealed that LThDP can be isolated as an intermediate, and it is hence unlikely that decarboxylation proceeds in barrierless fashion on the enzyme's active site. Further DFT analysis will be required to test the influence of the protein environment on the reaction coordinate of decarboxylation.

Although many chemical reactions were demonstrated to be stereoelectronically controlled or affected (*41*), much less is known about how enzymes employ stereoelectronic effects for catalysis. Dunathan proposed in the 1960s that pyridoxal phosphate-dependent enzymes, which are able to act differently on a given substrate (decarboxylation, transamination, and racemization), employ stereoelectronic effects to control the reaction specificity by aligning the incipient scissile bond perpendicular to the aldimine π-system (*42*). Accordingly, an overlap of the developing orbital and the extended cofactor orbitals accounts for lowering the energy of the transition state. Studies on numerous PLP-dependent enzymes have validated that reaction specificity in these enzymes is indeed stereoelectronically controlled (*43*). Our own studies on several ThDP enzymes could identify a similar modus operandi (*13*, *14*). Although ThDP enzymes are not able to catalyze an alternative elimination of different leaving groups of a given substrate as do PLP enzymes, the bond to be broken in pre-elimination intermediates is always aligned perpendicular to the π-system of the aromatic thiazolium ring, consistent with a maximum overlap mechanism. In our studies here, we could structurally characterize for the very first time a long-lived pre-elimination intermediate in which a 20−30° deviation from a perfect perpendicular (maximum overlap) alignment is observed. The elimination of CO_2 from this intermediate is kinetically compromised by a factor of 3000 when compared to that of the wild-type enzyme, for which perfect bond alignment is expected as previously observed in many other ThDP enzymes. A stronger stabilization of the nonperpendicular pre-elimination intermediate on the enzyme could be ruled out as the source of the kinetic effect, because a structurally related pre-elimination analogue is bound with the same affinity as in the wild-type enzyme. Consequently, the kinetic effect should reflect a strong stereoelectronic effect of the transition state of decarboxylation. To the best of our knowledge, this is one of the rare examples that allows estimation of the magnitude of a stereoelectronic effect in enzyme catalysis on the basis of structure−reactivity analysis of enzymic reaction intermediates.

ACKNOWLEDGMENT

We thank Ronald Duggleby for providing mutant plasmids. We acknowledge the Helmholtz-Zentrum Berlin-Electron storage ring BESSY II for provision of synchrotron radiation at beamline 14.2. The research leading to these results has received funding from the European Community's Seventh Framework Programme (FP7/2007-2013) under Grant 226716.

REFERENCES

1. Candy, J. M., and Duggleby, R. G. (1998) Structure and properties of pyruvate decarboxylase and site-directed mutagenesis of the *Zymomonas mobilis* enzyme. *Biochim. Biophys. Acta 1385*, 323–338.
2. Raj, K. C., Ingram, L. O., and Maupin-Furlow, J. A. (2001) Pyruvate decarboxylase: A key enzyme for the oxidative metabolism of lactic acid by *Acetobacter pasteurianus*. *Arch. Microbiol. 176*, 443–451.
3. Tittmann, K., Golbik, R., Uhlemann, K., Khailova, L., Schneider, G., Patel, M., Jordan, F., Chipman, D. M., Duggleby, R. G., and Hübner, G. (2003) NMR analysis of covalent intermediates in thiamin diphosphate enzymes. *Biochemistry 42*, 7885–7891.
4. Nemeria, N., Baykal, A., Joseph, E., Zhang, S., Yan, Y., Furey, W., and Jordan, F. (2004) Tetrahedral intermediates in thiamin diphosphate-dependent decarboxylations exist as a 1′,4′-imino tautomeric form of the coenzyme, unlike the Michaelis complex or the free coenzyme. *Biochemistry 43*, 6565–6575.
5. Schütz, A., Golbik, R., König, S., Hübner, G., and Tittmann, K. (2005) Intermediates and transition states in thiamin diphosphate-dependent decarboxylases. A kinetic and NMR study on wild-type indolepyruvate decarboxylase and variants using indolepyruvate, benzoylformate, and pyruvate as substrates. *Biochemistry 44*, 6164–6179.
6. Alvarez, F. J., Ermer, J., Hübner, G., Schellenberger, A., and Schowen, R. L. (1991) Catalytic Power of Pyruvate Decarboxylase: Rate-Limiting Events and Microscopic Rate Constants from Primary Carbon and Secondary Hydrogen Isotope Effects. *J. Am. Chem. Soc. 113*, 8402–8409.
7. Sun, S. X., Duggleby, R. G., and Schowen, R. L. (1995) Linkage of Catalysis and Regulation in Enzyme Action: Carbon-Isotope Effects, Solvent Isotope Effects, and Proton Inventories for the Unregulated Pyruvate Decarboxylase of *Zymomonas mobilis*. *J. Am. Chem. Soc. 117*, 7317–7322.
8. Nemeria, N. S., Chakraborty, S., Balakrishnan, A., and Jordan, F. (2009) Reaction mechanisms of thiamin diphosphate enzymes: Defining states of ionization and tautomerization of the cofactor at individual steps. *FEBS J. 276*, 2432–2446.
9. Nemeria, N., Chakraborty, S., Baykal, A., Korotchkina, L. G., Patel, M. S., and Jordan, F. (2007) The 1′,4′-iminopyrimidine tautomer of thiamin diphosphate is poised for catalysis in asymmetric active centers on enzymes. *Proc. Natl. Acad. Sci. U.S.A. 104*, 78–82.
10. Dobritzsch, D., König, S., Schneider, G., and Lu, G. G. (1998) High resolution crystal structure of pyruvate decarboxylase from *Zymomonas mobilis*: Implications for substrate activation in pyruvate decarboxylases. *J. Biol. Chem. 273*, 20196–20204.
11. Arjunan, P., Umland, T., Dyda, F., Swaminathan, S., Furey, W., Sax, M., Farrenkopf, B., Gao, Y., Zhang, D., and Jordan, F. (1996) Crystal structure of the thiamin diphosphate-dependent enzyme pyruvate decarboxylase from the yeast *Saccharomyces cerevisiae* at 2.3 angstrom resolution. *J. Mol. Biol. 256*, 590–600.
12. Wille, G., Meyer, D., Steinmetz, A., Hinze, E., Golbik, R., and Tittmann, K. (2006) The catalytic cycle of a thiamin diphosphate enzyme examined by cryocrystallography. *Nat. Chem. Biol. 2*, 324–328.
13. Tittmann, K., and Wille, G. (2009) X-ray crystallographic snapshots of reaction intermediates in pyruvate oxidase and transketolase illustrate common themes in thiamin catalysis. *J. Mol. Catal. B: Enzym. 61*, 93–99.
14. Kluger, R., and Tittmann, K. (2008) Thiamin diphosphate catalysis: Enzymic and nonenzymic covalent intermediates. *Chem. Rev. 108*, 1797–1833.

15. Candy, J. M., Koga, J., Nixon, P. F., and Duggleby, R. G. (1996) The role of residues glutamate-50 and phenylalanine-496 in *Zymomonas mobilis* pyruvate decarboxylase. *Biochem. J. 315*, 745–751.
16. Chang, A. K., Nixon, P. F., and Duggleby, R. G. (1999) Aspartate-27 and glutamate-473 are involved in catalysis by *Zymomonas mobilis* pyruvate decarboxylase. *Biochem. J. 339*, 255–260.
17. Liu, M., Sergienko, E. A., Guo, F. S., Wang, J., Tittmann, K., Hübner, G., Furey, W., and Jordan, F. (2001) Catalytic acid-base groups in yeast pyruvate decarboxylase. 1. Site-directed mutagenesis and steady-state kinetic studies on the enzyme with the D28A, H114F, H115F, and E477Q substitutions. *Biochemistry 40*, 7355–7368.
18. Baillie, A. C., Wright, B. J., and Wright, K. (1982) U.S. Patent 4,339,443.
19. Kluger, R., and Pike, D. C. (1977) Active-Site Generated Analogs of Reactive Intermediates in Enzymic Reactions: Potent Inhibition of Pyruvate Dehydrogenase by a Phosphonate Analog of Pyruvate. *J. Am. Chem. Soc. 99*, 4504–4506.
20. Huang, C. Y., Chang, A. K., Nixon, P. F., and Duggleby, R. G. (2001) Site-directed mutagenesis of the ionizable groups in the active site of *Zymomonas mobilis* pyruvate decarboxylase: Effect on activity and pH dependence. *Eur. J. Biochem. 268*, 3558–3565.
21. Nemeria, N. S., Korotchkina, L. G., Chakraborty, S., Patel, M. S., and Jordan, F. (2006) Acetylphosphinate is the most potent mechanism-based substrate-like inhibitor of both the human and *Escherichia coli* pyruvate dehydrogenase components of the pyruvate dehydrogenase complex. *Bioorg. Chem. 34*, 362–379.
22. Kern, D., Kern, G., Neef, H., Tittmann, K., KillenbergJabs, M., Wikner, C., Schneider, G., and Hübner, G. (1997) How thiamine diphosphate is activated in enzymes. *Science 275*, 67–70.
23. Kabsch, W. (1993) Automatic Processing of Rotation Diffraction Data from Crystals of Initially Unknown Symmetry and Cell Constants. *J. Appl. Crystallogr. 26*, 795–800.
24. Collaborative Computational Project Number 4 (1994) The CCP4 suite: Programs for protein crystallography. *Acta Crystallogr. D50*, 760–763.
25. Brünger, A. T., Adams, P. D., Clore, G. M., DeLano, W. L., Gros, P., Grosse-Kunstleve, R. W., Jiang, J. S., Kuszewski, J., Nilges, M., Pannu, N. S., Read, R. J., Rice, L. M., Simonson, T., and Warren, G. L. (1998) Crystallography & NMR system: A new software suite for macromolecular structure determination. *Acta Crystallogr. D54*, 905–921.
26. Adams, P. D., Grosse-Kunstleve, R. W., Hung, L. W., Ioerger, T. R., McCoy, A. J., Moriarty, N. W., Read, R. J., Sacchettini, J. C., Sauter, N. K., and Terwilliger, T. C. (2002) PHENIX: Building new software for automated crystallographic structure determination. *Acta Crystallogr. D58*, 1948–1954.
27. Emsley, P., and Cowtan, K. (2004) Coot: Model-building tools for molecular graphics. *Acta Crystallogr. D60*, 2126–2132.
28. Davis, I. W., Leaver-Fay, A., Chen, V. B., Block, J. N., Kapral, G. J., Wang, X., Murray, L. W., Arendall, W. B., Snoeyink, J., Richardson, J. S., and Richardson, D. C. (2007) MolProbity: Sll-atom contacts and structure validation for proteins and nucleic acids. *Nucleic Acids Res. 35*, W375–W383.
29. Frisch, M. J., Trucks, G. W., Schlegel, H. B., Scuseria, G. E., Robb, M. A., Cheeseman, J. R., Montgomery, J. A., Jr., Vreven, T., Kudin, K. N., Burant, J. C., Millam, J. M., Iyengar, S. S., Tomasi, J., Barone, V., Mennucci, B., Cossi, M., Scalmani, G., Rega, N., Petersson, G. A., Nakatsuji, H., Hada, M., Ehara, M., Toyota, K., Fukuda, R., Hasegawa, J., Ishida, M., Nakajima, T., Honda, Y., Kitao, O., Nakai, H., Klene, M., Li, X., Knox, J. E., Hratchian, H. P., Cross, J. B., Bakken, V., Adamo, C., Jaramillo, J., Gomperts, R., Stratmann, R. E., Yazyev, O., Austin, A. J., Cammi, R., Pomelli, C., Ochterski, J. W., Ayala, P. Y., Morokuma, K., Voth, G. A., Salvador, P., Dannenberg, J. J., Zakrzewski, V. G., Dapprich, S., Daniels, A. D., Strain, M. C., Farkas, O., Malick, D. K., Rabuck, A. D., Raghavachari, K., Foresman, J. B., Ortiz, J. V., Cui, Q., Baboul, A. G., Clifford, S., Cioslowski, J., Stefanov, B. B., Liu, G., Liashenko, A., Piskorz, P., Komaromi, I., Martin, R. L., Fox, D. J., Keith, T., Al-Laham, M. A., Peng, C. Y., Nanayakkara, A., Challacombe, M., Gill, P. M. W., Johnson, B., Chen, W., Wong, M. W., Gonzalez, C., and Pople, J. A. (2005) Gaussian 03, revision D.1, Gaussian, Inc., Wallingford, CT.
30. Friedemann, R., Tittmann, K., Golbik, R., and Hübner, G. (2009) DFT and MP2 studies on the C2-C2α bond cleavage in thiamin catalysis. *J. Mol. Catal. B: Enzym. 61*, 36–38.
31. Barletta, G., Huskey, W. P., and Jordan, F. (1992) Observation of a 2-α-Enamine from a 2-(Methoxyphenylmethyl)-3,4-dimethylthiazolium Salt in Water: Implications for Catalysis by Thiamin Diphosphate-Dependent α-Keto Acid Decarboxylases. *J. Am. Chem. Soc. 114*, 7607–7608.
32. Arjunan, P., Sax, M., Brunskill, A., Chandrasekhar, K., Nemeria, N., Zhang, S., Jordan, F., and Furey, W. (2006) A thiamin-bound, pre-decarboxylation reaction intermediate analogue in the pyruvate dehydrogenase E1 subunit induces large scale disorder-to-order transformations in the enzyme and reveals novel structural features in the covalently bound adduct. *J. Biol. Chem. 281*, 15296–15303.
33. Asztalos, P., Parthier, C., Golbik, R., Kleinschmidt, M., Hübner, G., Weiss, M. S., Friedemann, R., Wille, G., and Tittmann, K. (2007) Strain and near attack conformers in enzymic thiamin catalysis: X-ray crystallographic snapshots of bacterial transketolase in covalent complex with donor ketoses xylulose 5-phosphate and fructose 6-phosphate, and in noncovalent complex with acceptor aldose ribose 5-phosphate. *Biochemistry 46*, 12037–12052.
34. Brandt, G. S., Nemeria, N., Chakraborty, S., McLeish, M. J., Yep, A., Kenyon, G. L., Petsko, G. A., Jordan, F., and Ringe, D. (2008) Probing the active center of benzaldehyde lyase with substitutions and the pseudosubstrate analogue benzoylphosphonic acid methyl ester. *Biochemistry 47*, 7734–7743.
35. Brandt, G. S., Kneen, M. M., Chakraborty, S., Baykal, A. T., Nemeria, N., Yep, A., Ruby, D. I., Petsko, G. A., Kenyon, G. L., McLeish, M. J., Jordan, F., and Ringe, D. (2009) Snapshot of a Reaction Intermediate: Analysis of Benzoylformate Decarboxylase in Complex with a Benzoylphosphonate Inhibitor. *Biochemistry 48*, 3247–3257.
36. Bruning, M., Berheide, M., Meyer, D., Golbik, R., Bartunik, H., Liese, A., and Tittmann, K. (2009) Structural and Kinetic Studies on Native Intermediates and an Intermediate Analogue in Benzoylformate Decarboxylase Reveal a Least Motion Mechanism with an Unprecedented Short-Lived Predecarboxylation Intermediate. *Biochemistry 48*, 3258–3268.
37. Nemeria, N., Korotchkina, L., McLeish, M. J., Kenyon, G. L., Patel, M. S., and Jordan, F. (2007) Elucidation of the chemistry of enzyme-bound thiamin diphosphate prior to substrate binding: Defining internal equilibria among tautomeric and ionization states. *Biochemistry 46*, 10739–10744.
38. Wu, N., Mo, Y. R., Gao, J. L., and Pai, E. F. (2000) Electrostatic stress in catalysis: Structure and mechanism of the enzyme orotidine monophosphate decarboxylase. *Proc. Natl. Acad. Sci. U.S.A. 97*, 2017–2022.
39. Kluger, R., Ikeda, G., Hu, Q. Y., Cao, P. P., and Drewry, J. (2006) Accelerating unimolecular decarboxylation by preassociated acid catalysis in thiamin-derived intermediates: Implicating Bronsted acids as carbanion traps in enzymes. *J. Am. Chem. Soc. 128*, 15856–15864.
40. Kluger, R., and Rathgeber, S. (2008) Catalyzing separation of carbon dioxide in thiamin diphosphate-promoted decarboxylation. *FEBS J. 275*, 6089–6100.
41. Deslongchamps, P. (1983) Stereoelectronic Effects in Organic Chemistry, Pergamon Press, New York.
42. Dunathan, H. C. (1966) Conformation and Reaction Specificity in Pyridoxal Phosphate Enzymes. *Proc. Natl. Acad. Sci. U.S.A. 55*, 712–716.
43. Toney, M. D. (2005) Reaction specificity in pyridoxal phosphate enzymes. *Arch. Biochem. Biophys. 433*, 279–287.